

Reactivity on Deprotonation

Reactivity of Me-pma Rh^I and Ir^I Complexes upon Deprotonation and Their Application in Catalytic Carbene Carbonylation Reactions

Zhou Tang,^[a] Cristina Tejel,^[b] Marc Martinez de Sarasa Buchaca,^[a,b] Martin Lutz,^[c] Jarl Ivar van der Vlugt,^[a] and Bas de Bruin*^[a]

Dedicated to Luis Oro on the occasion of his 70th birthday

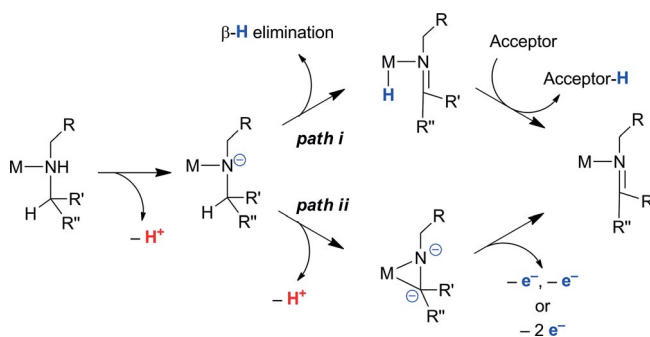
Abstract: Dehydrogenative oxidation of amines is a relevant process in metal-mediated catalysis, with the amines being either substrates or ligands. Transformation of amine- into imine-type ligands in the coordination sphere of a transition metal can be an important catalyst activation process. The behaviour of secondary pyridin-2-ylmethanamine (pma) ligands in the corresponding rhodium and iridium complexes upon NH deprotonation varies, depending on a number of factors. In this paper the behaviour of the Me-pma ligand [Me-pma = *N*-methyl-1-(pyridin-2-yl)methanamine] bound to [Rh(cod)]⁺ and [Ir(cod)]⁺ was studied. Whereas the iridium amido complex could be ob-

tained upon NH deprotonation, the rhodium complex instantaneously disproportionated into a free pma ligand and an unusual dinuclear complex, adopting a structure with two Rh^I metal centres hosted by a dianionic (pma-2H)²⁻ ligand, and with the ligand coordinating to Rh₂ as an “aza-allyl” fragment. The study gives further proof for the effect of pyridine ligation on the previously observed charge-transfer from the ligand to the metal. Furthermore, the catalytic activity of both the Ir and the Rh species with Me-pma in carbene carbonylation reactions to generate ketenes was studied.

Introduction

Dehydrogenative oxidation of amines is an important process in both biological and chemical systems.^[1] Amine oxidases are widely found in bacteria, plants and animals, and are involved in a number of basic biological processes, such as lysyl oxidation in the cross-linking of collagen.^[2] Transition-metal-promoted dehydrogenative amine oxidation reactions are frequently used in synthetic chemistry to generate imines,^[3] nitriles^[4] and diazo compounds.^[5] Transformation of amine- into imine-type ligands in the coordination sphere of transition metals can also be an important catalyst activation process.^[6] These reactions involve multiple proton- and electron-transfer steps, but the mechanisms are not fully understood at the molecular level. Metal-amido complexes are usually key intermediates in these transformations, irrespective of the pathway involved. For

oxidation of a metal-bound amido group into the corresponding imine, two distinct pathways are generally proposed to be operational (Scheme 1). The first involves a metal-hydride intermediate arising from β-H elimination, which can subsequently be transferred to a hydrogen acceptor^[7] or released in the form of dihydrogen (path i);^[8] the second does not involve a metal-hydride intermediate but proceeds through (stepwise or concerted) deprotonation and oxidation steps (one proton and two electrons), reducing either the metal or an exogenous “oxidant”^[9] (path ii). Other mechanisms involving either direct ligand-to-(exogenous) substrate hydride-transfer^[10] or H-atom transfer^[11] are also reported.



Scheme 1. Two generalized proposed pathways for imine formation via metal-amido complexes.

[a] *Homogeneous, Bioinspired & Supramolecular Catalysis, van 't Hoff Institute for Molecular Sciences, Faculty of Sciences, University of Amsterdam, Science Park 904, 1098 XH Amsterdam, The Netherlands*
E-mail: b.debruin@uva.nl
www.homkat.nl

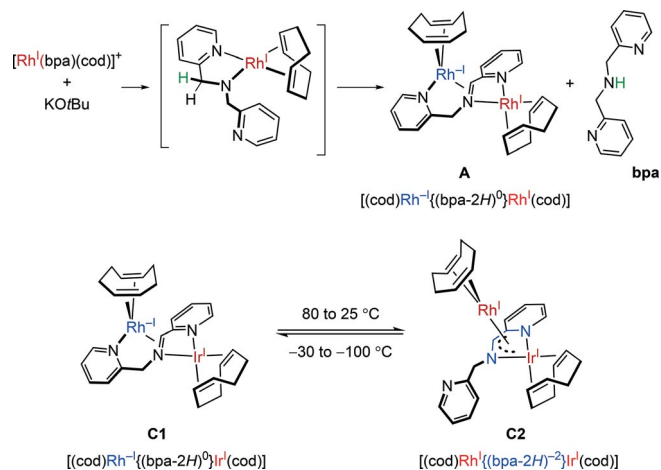
[b] *Departamento de Química Inorgánica, Instituto de Síntesis Química y Catálisis Homogénea – ISQCH, CSIC – Universidad de Zaragoza, Pedro Cerbuna 12, 50009 Zaragoza, Spain*

[c] *Crystal & Structural Chemistry, Bijvoet Center for Biomolecular Research, Utrecht University, Padualaan 8, 3584 CH Utrecht, The Netherlands*

Supporting information and ORCID(s) from the author(s) for this article are available on the WWW under <http://dx.doi.org/10.1002/ejic.201501302>.

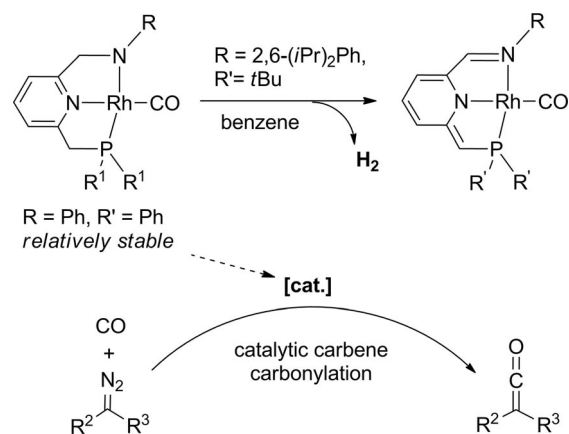
Ligand-based redox activity^[12] adds to the complexity of the overall system and the mechanistic interpretation of amine to imine conversion, because the ligand can participate directly in the redox process.^[13] For example, one-electron oxidation of an amido-rhodium complex $[\text{Rh}^{\text{I}}(\text{bipy})(\text{trop}_2\text{N})]$ ($\text{trop} = 5\text{-H-di-benzo}[a,d]\text{cycloheptene-5-yl}$, $\text{bipy} = 2,2'\text{-bipyridyl}$) led to formation of a rhodium aminyl radical $[\text{Rh}^{\text{I}}(\text{bipy})(\text{trop}_2\text{N})]\text{OTf}$ ($\text{OTf}^- = \text{trifluorosulfonate}$) instead of the expected rhodium(II) complex, because the oxidation occurs mainly at the amido ligand.^[14a,14b] Mono-deprotonation of a metal-bound amino group can also trigger formation of a ruthenium aminyl radical $[\text{Ru}^{\text{II}}(\text{Bu}_2\text{sq})\text{-}(\text{LNH})]$ [$\text{LNH}_2 = \text{bis}(2\text{-pyridylmethyl})\text{-2-aminoethylamine}$, $\text{Bu}_2\text{sq} = 3,5\text{-di-tert-butylsemiquinonate}$] from its amido electroisomer, which is able to catalyse the oxidation of alcohols into aldehydes.^[14c,14d] Two-electron oxidation of a metal-bound amido ligand is usually accompanied by proton loss from the α -position to the nitrogen, producing an imine complex (which is often more stable, in particular for late transition metals). Previous studies investigated the dehydrogenative oxidation of rhodium and iridium amino complexes derived from cationic $[\text{Rh}^{\text{I}}(\text{bpa})(\text{cod})]^+$ and $[\text{Ir}^{\text{I}}(\text{bpa})(\text{cod})]^+$ [$\text{bpa} = \text{Py-CH}_2\text{-NH-CH}_2\text{-Py} = \text{bis}(\text{pyridin-2-ylmethyl})\text{amine}$, $\text{cod} = 1,5\text{-cyclooctadiene}$].^[15] This has led to the mixed-valent dirhodium complex $[(\text{cod})\text{Rh}^{\text{I}}\{(\text{bpa-2H})^0\}\text{Rh}^{\text{I}}(\text{cod})]$ (**A**, Scheme 2), which was obtained by deprotonation of the mononuclear cationic amino-precursor $[\text{Rh}^{\text{I}}(\text{bpa})(\text{cod})]^+$ with one molar equivalent of base. The reaction likely involves an unstable amido complex as intermediate. The overall reaction at the ditopic ligand of complex **A** consists of two deprotonations and a two-electron transfer process, leading to formation of the neutral $\text{Py-CH}_2\text{-N=CH-Py}$ imine ligand $(\text{bpa-2H})^0$ with formal reduction of one of the metal centres from rhodium(I) to rhodium(-I) (Scheme 2).^[15b] The analogous dinuclear rhodium(norbornadiene) complex **B**,^[15a] and a heterodinuclear rhodium-iridium complex **C1**,^[15b,15c] with similar electronic structures, were also fully characterised. Interestingly, complex **C1** $[(\text{cod})\text{Rh}^{\text{I}}\{(\text{bpa-2H})^0\}\text{Ir}^{\text{I}}(\text{cod})]$ was observed in equilibrium with isomer **C2**, which holds the formulation of $[(\text{cod})\text{Rh}^{\text{I}}\{(\text{bpa-2H})^{-2}\}\text{Ir}^{\text{I}}(\text{cod})]$. Key structural changes on going from **C1** to **C2** (Scheme 2) were decoordination of one of the pyridyl ligands and a slight slippage of Rh in order to interact with the "iridaazabutenyl" moiety (Scheme 2). These changes are associated with two-electron transfer from the rhodium to the "imine" moiety of the ligand. Moreover, (de)coordination of the pendant pyridyl ring may be directly related to reversible metal-to-ligand charge-transfer, because pyridine coordination is likely required to stabilise the reduced tetrahedral $\text{Rh}^{-\text{I}}$ centre.

Besides the reactions described above (Scheme 1), spontaneous H_2 -loss from a protic and hydridic ligand-arm of PNN-pincer-type ligands has also been observed to occur in apolar solvents such as benzene,^[15e] which triggered interesting ligand-centred reactivity (Scheme 3) that goes beyond chemistry with, for example, PNP or bipyridine-based PNN ligands.^[16] Interestingly, the ligand substituents and/or the solvent seem to play a crucial role in this process, because the amido form of PNN-ligands of the type shown in Scheme 3 proved to be much more stable in tetrahydrofuran (THF), with no indications for spontaneous H_2 -loss from these related ligands.^[6a,17] We re-



Scheme 2. Top: previous work on mixed-valent dinuclear rhodium complex **A** obtained through cooperative double deprotonation and ligand-to-metal charge transfer.^[15b] Bottom: isomerisation of complex **C** to the two extreme electronic forms **C1** and **C2**, affected by temperature.^[15c]

cently also demonstrated that those amido complexes are active catalysts in catalytic carbene carbonylation reactions to produce ketenes (Scheme 3).^[18]



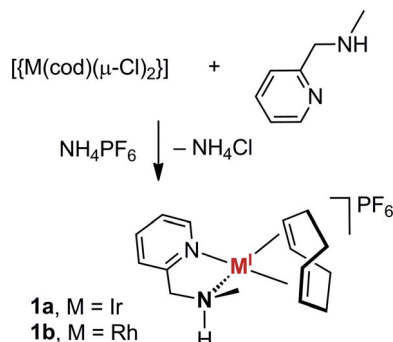
Scheme 3. Top: H_2 loss from a Rh-PNN amido complex. Bottom: A Rh-PNN amido complex as the catalyst for carbene carbonylation reaction to produce ketenes.^[15e]

To elucidate the subtleties involved in the coordination chemistry and (catalytic) reactivity of pyridyl-amido complexes of Rh and Ir, as well as pyridyl-imine ligands involving two metal centres, we herein report on rhodium and iridium(cod) complexes based on the Me-pma ligand [$\text{Me-pma} = N\text{-methyl-1-(pyridin-2-yl)methanamine}$], an analogue to the bpa ligand that lacks the pendant pyridine. The aim of these studies was to investigate the effect of the Me-pma ligand on the dehydrogenative ligand oxidation process and to shed more light on the effect of pyridine ligation on the previously observed charge-transfer from the ligand to the metal (Scheme 2, bottom). We further evaluated their activity in catalytic carbene carbonylation.

Results and Discussion

The mononuclear complexes **1a** (Ir) and **1b** (Rh) were prepared in good yields (87 and 81 % yield, respectively) according to a

previously reported procedure (Scheme 4),^[15b] reacting the Me-pma ligand with the $[[M(\text{cod})(\mu\text{-Cl})_2]]$ precursors ($M = \text{Ir}^I$ or Rh^I), followed by precipitation of the complexes as PF_6^- salts by adding NH_4PF_6 . In the ^1H NMR spectrum, the $-\text{NH}$ signals of complexes **1a** and **1b** appear at $\delta = 4.32$ and 3.76 ppm, respectively. The methylene group in both complexes is observed as a well-defined doublet of doublet (AB spin system), implying inequivalence of the two protons. Similarly, asymmetry is observed for the cyclooctadiene ligands. Single crystals of both complexes suitable for X-ray diffraction studies were obtained by top-layering pentane onto concentrated dichloromethane solutions.



Scheme 4. Synthesis of complexes **1a** and **1b**.

The crystal structures of **1a** and **1b** (Figure 1) are isomorphous and the two metal centres consequently exhibit almost identical square planar geometries with the plane defined by the two nitrogen atoms of the Me-pma ligand and the two centroids of the C=C bonds coordinated to the metal. The geometry around atom N2 is tetrahedral in both cases, with the lone pair coordinated to the metal and the methyl group pointing away from and being almost perpendicular to the coordination planes of the metals [$\angle \text{Ct1-Ct2-N2-C7}$ $98.10(16)$ and $99.46(11)^\circ$ for **1a** and **1b**, respectively]. The M–N and M–Ct bonds are slightly more contracted for the iridium complex **1a**.

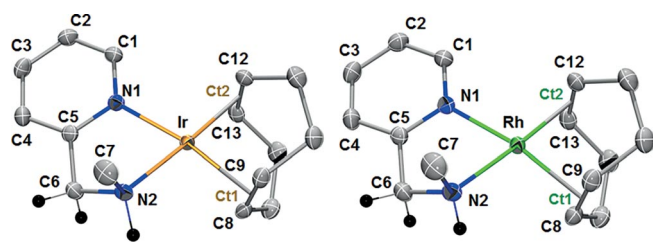
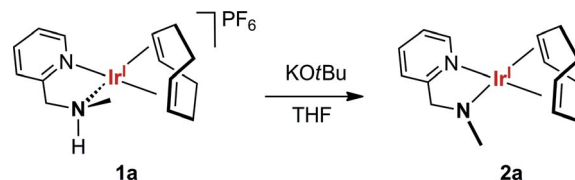


Figure 1. Molecular structure (ORTEP at 50 % level) of the cations of complexes **1a** (left) and **1b** (right). Hydrogen atoms are removed for clarity, except for those on C6 and N2; red dots represent the centroids of the coordinated C=C bonds of the cod ligand. Selected bond lengths [Å] and angles [°], for **1a**: Ir–N1, 2.0814(19); Ir–N2, 2.1044(19); Ir–Ct1, 2.0012(17); Ir–Ct2, 2.0083(15); N1–C1, 1.353(3); N1–C5, 1.353(3); C5–C6, 1.502(3); C6–N2, 1.495(3); C8–C9, 1.410(3); C12–C13, 1.412(3); N1–Ir–Ct1, 170.02(7); N2–Ir–Ct2, 176.57(7); N1–Ir–N2, 79.21(7); Ct1–Ir–Ct2, 87.57(7); Ir–N2–C6, 107.08(14); Ct1–Ct2–N2–C7, 98.10(16). For **1b**: Rh–N1, 2.0965(12); Rh–N2, 2.1147(13); Rh–Ct1, 2.0143(11); Rh–Ct2, 2.0210(10); N1–C1, 1.3497(19); N1–C5, 1.3542(18); C5–C6, 1.503(2); C6–N2, 1.485(2); C8–C9, 1.397(2); C12–C13, 1.392(2); N1–Rh–Ct1, 169.86(4); N2–Rh–Ct2, 176.36(5); N1–Rh–N2, 79.29(5); Ct1–Rh–Ct2, 87.89(4); Rh–N2–C6, 106.40(9); Ct1–Ct2–N2–C7, 99.46(11).

Synthesis of Iridium–Amido Complex **2a** Involving Monodeprotonation of **1a**

Addition of one equivalent of potassium *tert*-butoxide (KOtBu) to a THF solution of **1a** led to a colour change from yellow to deep-red. Disappearance of the $-\text{NH}$ signal, appearance of the methylene group as a singlet at $\delta = 4.55$ ppm and chemical shifts for the cod signals ($\Delta\delta = 0.39$ – 0.27 ppm upfield relative to **1a**) in the ^1H NMR spectrum support the formation of the neutral iridium-amido complex **2a** (Scheme 5).



Scheme 5. Synthesis of complex **2a** by monodeprotonation with KOtBu.

Single crystals suitable for X-ray structure determination were obtained by storing a concentrated diethyl ether solution of **2a** at -20°C . The molecular structure of deprotonated complex **2a** reveals a square-planar coordination geometry around iridium (Figure 2). In contrast to the neutral ligands in **1a** and **1b**, the anionic ligand of **2a** coordinates in the coordination plane without remarkable distortion ($\angle \text{Ir-N1-C5-C6}$: 5.26° ; $\angle \text{N1-C5-C6-N2}$: 1.18°). The Ir–N2 bond in **2a** is shortened from 2.1043(19) Å in **1a** to 1.9730(13) Å, resulting from a stabilising push-pull π -interaction. The nitrogen lone pair donates to the metal, which, in turn, back-donates to the *trans*-C=C bond of the cod-ligand. Hence, the C12–C13 bond length of the cod ligand *trans* to the amido N atom is elongated to 1.427(2) Å compared with the corresponding bond in **1a** [1.412(4) Å], and is also longer than C8–C9 [1.412(2) Å], in agreement with enhanced π -back-donation from the metal upon deprotonation of the secondary amine nitrogen.

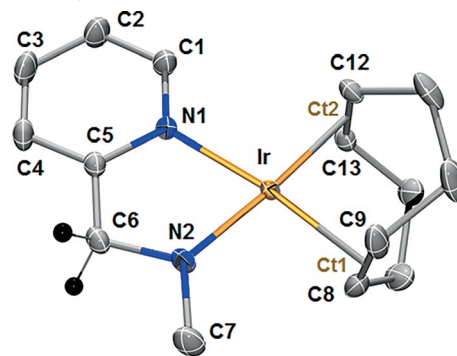
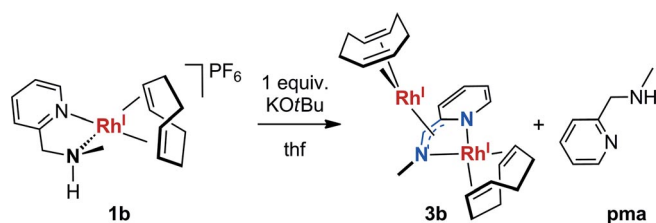


Figure 2. Molecular structure (ORTEP at 50 % level) of **2a**. Hydrogen atoms are removed for clarity, except on C6. Selected bond lengths [Å] and angles [°]: Ir–N1, 2.0901(12); Ir–N2, 1.9730(13); Ir–Ct1, 1.992; Ir–Ct2, 1.994; N1–C1, 1.349(2); N1–C5, 1.3493(19); C5–C6, 1.490(2); C6–N2, 1.436(2); N2–C7, 1.449(2); C8–C9, 1.412(4); C12–C13, 1.427(2); N1–Ir–Ct1, 172.62; N2–Ir–Ct2, 175.91; N1–Ir–N2, 79.78(5); Ct1–Ir–Ct2, 87.43; Ir–N1–C5–C6, 5.26; N1–C5–C6–N2, -1.18 .

Synthesis of the Bimetallic Complex **3b** Involving Cooperative Ligand Deprotonation

In contrast to the mono-deprotonation of iridium complex **1a**, treatment of the rhodium complex **1b** in $[\text{D}_8]\text{THF}$ with one mo-

lar equivalent of KOtBu did not produce the rhodium-amido complex **2b** (Scheme 6). Instead, spontaneous double deprotonation was observed, despite using only one equivalent of base. In the ^1H NMR spectrum (see the Supporting Information, Figure S1), half an equivalent of free Me-pma ligand was detected, and the pyridine signals of the remaining Me-pma ligand were remarkably shifted upfield to the region of $\delta = 6.71\text{--}5.84$ ppm. The same chemical shift trend was observed for the cod signals (especially the vinylic protons), compared with those in complex **1b**, indicating the electron-rich nature of the new rhodium complex **3b**. Integration of the peaks in the ^1H NMR spectrum points to the presence of two cod ligands (which is suggestive of the presence of two rhodium centres) and one ligand derived from Me-pma. However, signals corresponding to the NH or CH_2 moieties of the original Me-pma ligand were absent, and instead one sharp *pseudo*-triplet^[19] at $\delta = 5.52$ ppm (1 H) was found that did not seem to correlate with other hydrogen nuclei in the $^1\text{H},^1\text{H}$ -cosy spectrum. The observed reactivity pattern resembles that of the previously reported reaction of complex $[\text{Rh}(\text{bpa})(\text{cod})]\text{PF}_6$ with one equivalent of KOtBu, resulting in formation of the dinuclear mixed-valent $\{\text{Rh}^{\text{I}}, \text{Rh}^{\text{-I}}\}$ complex **A** $[(\text{cod})\text{Rh}^{\text{I}}\{(\text{bpa}-2\text{H})^{-2}\}-\text{Rh}^{\text{-I}}(\text{cod})]$,^[15b] which overall shows an interesting pathway for the dehydrogenative oxidation of a metal-bound amine into an imine (Scheme 2).



Scheme 6. Synthesis of complex **3b** by treating **1b** with one equivalent of KOtBu.

The new dinuclear species **3b**, formulated as $[(\text{cod})\text{Rh}^{\text{I}}\{(\text{Me-pma}-2\text{H})^{-2}\}\text{Rh}^{\text{-I}}(\text{cod})]$, was assigned to contain the “doubly deprotonated” dianionic $\{(\text{Me-pma}-2\text{H})^{-2}\}$ ligand. Complex **3b** was also efficiently synthesised by reacting $[(\text{Rh}(\text{cod})(\mu\text{-OMe}))_2]$ with Me-pma in a 1:1 molar ratio. In this case, the bridging methoxy ligand in the precursor complex functions as an internal base. Further recrystallisation afforded **3b** as a dark brownish-red solid in 62 % yield.

Double deprotonation of the Me-pma ligand converts the “ $\text{CH}_2\text{-NHMe}$ ” moiety into a dianionic “ $(\text{CH-NHMe})^{2-}$ ” moiety. Subsequent two-electron oxidation of the $(\text{Me-pma}-2\text{H})^{2-}$ would transform the ligand into a neutral $(\text{Me-pma}-2\text{H})^0$ ligand containing an imine “ C(H)=NMe ” moiety. In case of complexes **A** and **B**, based on the bpa ligand (see Scheme 2 and surrounding discussion in the introduction), as well as for their iridium analogues, deprotonation leads to imine formation. This conversion was observed in an intramolecular redox process wherein one of the metal ions acts as a two-electron oxidant, thus producing species that are best described as having a π -bound imine ligand coordinated to a tetrahedral rhodium(–I) or iridium(–I) ion, respectively. To determine whether the same situation could arise in complex **3b**, the spectral and structural parameters of this complex were examined in detail. The pyridine proton sig-

nals of **3b** in C_6D_6 appear in the range between $\delta = 6.57\text{--}5.66$ ppm in the ^1H NMR spectrum. The triplet signal at $\delta = 5.16$ ppm ($J = 0.8$ Hz) correlates with a doublet at $\delta = 89.80$ ppm ($J_{\text{C,H}} = 5.5$ Hz) in the $^1\text{H},^{13}\text{C}$ -hsqc spectrum, and it is assigned to the “imine” HC=N proton. Both signals of the imine moiety are markedly shifted downfield compared with those of complexes **A** and **B** (^1H : $\delta = 3.54$ and 4.33 ppm, ^{13}C : $\delta = 76.9$ and 81.88 ppm, respectively), pointing to a stronger “imine” character of the C=N bond in **3b** and therefore a higher degree of electron-transfer from the deprotonated N2-C6 moiety (see Table 1). However, oxidation of the dianionic “ $(\text{CH-NHMe})^{2-}$ ” moiety to form a neutral C(H)=NMe imino moiety could occur either by electron-transfer from the ligand to the metal, with the Rh^{I} centre as the formal oxidant, as observed for **A** and **B** (Scheme 2), or by charge-delocalisation into the pyridine moiety, with the aromatic ring acting as the electron acceptor. The latter is more likely for **3b**, because the pyridine proton signals of **3b** are markedly shifted upfield relative to complexes **A** and **B** (see shifts of H_{Py} in Table 1). Furthermore, the absence of a pendant coordinating pyridine group in **3b** should destabilise a hypothetical $\text{Rh}^{\text{-I}}$ centre, because a tetrahedral geometry is no longer accessible. Three sharp signals in the region of $\delta = 4.23\text{--}3.42$ ppm (four H atoms) are assigned to the olefinic protons of $[\text{cod}(1)]$ coordinated to Rh1 on the pma ligand plane. Signals at $\delta = 2.06\text{--}1.94$ and $1.85\text{--}1.75$ ppm are assigned to the allylic protons of this $[\text{cod}(1)]$ -ligand, based on $^1\text{H},^{13}\text{C}$ -hsqc, $^1\text{H},^1\text{H}$ -cosy and $^1\text{H},^1\text{H}$ -noesy spectra, which all indicate the absence of any symmetry in $[\text{cod}(1)]$. In contrast, the olefinic protons of $[\text{cod}(2)]$ above the Me-pma-2H ligand plane give rise to a very broad signal in the range of $4.98\text{--}3.76$ ppm, whereas the corresponding carbon signals are not visible in the ^{13}C NMR spectrum and the allylic proton signals show up as three sets of multiplets in a more narrow region of $\delta = 2.26\text{--}1.79$ ppm in the ^1H NMR spectrum. The observed coalescence of the olefinic cod signals of $[\text{cod}(2)]$ points to rotation of this ligand around the Rh2 centre with an intermediate rate on the NMR timescale at room temperature. In fact, $[\text{cod}(2)]$ rotation around Rh2 is slower than observed for complex **A**, but still faster than $[\text{cod}(1)]$ rotation around Rh1 . This may indicate some “tetrahedral character” for Rh2 ,^[15b,20] but the unsaturated nature of Rh2 (lacking an additional donor from a pendant pyridine such as in complexes **A** and **C1**) might also contribute to the rotational fluxionality of $[\text{cod}(2)]$ being faster than $[\text{cod}(1)]$.

Table 1. Selected NMR parameters [δ (ppm)] of known complexes **A**,^[15b] **B**,^[15a] **C1**^[15c] and **C2**^[15c] (see Scheme 2) compared with those of new complex **3b**.

δ	A	B	C1	C2 ^[a]	3b
$\text{H}_{\text{HC=N}}$	4.33	3.54	4.84	5.77	5.16
$\text{C}_{\text{HC=N}}$ ($J_{\text{Rh,C}}$)	82.2 (7)	76.9 (9)	91.8 (br) ^[b]	93.3 (5)	89.8 (5)
H_{Py1}	6.80	6.95	6.94 ^[c]	6.95	6.56
H_{Py3}	6.58	6.56	6.90 ^[c]	6.52	6.47
H_{Py4}	6.20	6.41	7.35 ^[c]	6.38	6.16
H_{Py2}	5.78	5.65	6.48 ^[c]	5.81	5.68

[a] At 80 °C. [b] At –70 °C. [c] At –100 °C.

Deep-red crystals of **3b** suitable for X-ray diffraction studies were obtained from diethyl ether at –20 °C (Figure 3, left). The structure contains two $\text{Rh}(\text{cod})$ fragments and a ditopic doubly

deprotonated Me-pma ligand. Atom Rh1 is clearly coordinated to the two nitrogen atoms (N1 and N2) and to the cod ligand, resulting in a square-planar environment as expected for rhodium(+I). However, the geometry around Rh2 is more difficult to define because, in addition to the cod ligand, it seems to have an interaction with the N2–C6–C5 moiety,^[21] and also interacts weakly with Rh1 as indicated by the relatively short Rh1–Rh2 bond length of 2.91468(19) Å (Table 2 and Table 3, Figure 3). Nonetheless, key parameters to define the oxidation state for this rhodium atom were the intraligand bond lengths in the α -pyridylamine moiety (Table 2), which clearly indicates it to be closer to **C2** than to complexes **A/B**, both having an oxidised (bpa-2H)⁰ ligand; for example, the N1–C5, C5–C4 and C4–C3 bond lengths of **3b** are 1.385(2), 1.421(5) and 1.356(7) Å, respectively, indicating alternating double and single bond characters, similar to 1.394(5), 1.421(5) and 1.356(7) Å for **C2**.

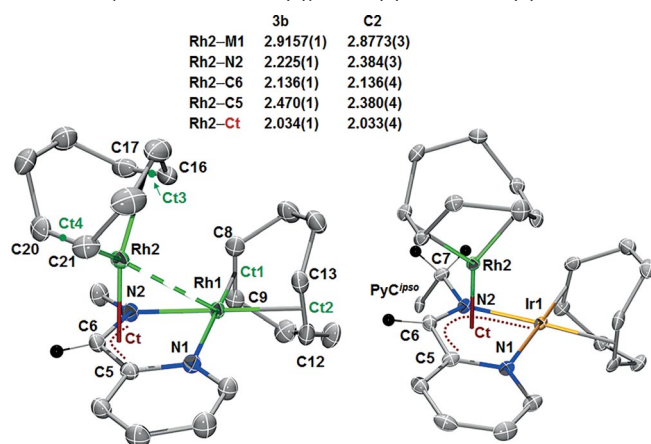


Figure 3. Molecular structure (ORTEP at 50% level) of **3b** and **C2**. Hydrogen atoms are removed for clarity, except on C6 and C7. Selected bond lengths [Å] and angles [°], for **3b**: Rh1–N1, 2.0711(14); Rh1–N2, 2.0340(14); Rh1–Ct1, 2.0031(13); Rh1–Ct2, 2.0016(12); C8–C9, 1.403(3); C12–C13, 1.403(3); Rh2–Ct3, 2.0259(14); Rh2–Ct4, 2.0004(13); C16–C17, 1.391(3); C20–C21, 1.397(3); N1–Rh1–Ct1, 170.61(6); N2–Rh1–Ct2, 175.65(6); N1–Rh1–N2, 79.73(5); Ct1–Rh1–Ct2, 87.77(5); Ct4–Rh2–Rh1, 159.52(4); Ct3–Rh2–Ct4, 87.87(6).

Table 2. Selected interligand bond lengths [Å] of complexes **A**,^[15b] **B**,^[15a] **C2**^[15c] and **3b**.

	A	B	3b	C2
N1–C5	1.373(3)	1.362(4)	1.385(2)	1.394(5)
C5–C6	1.435(4)	1.437(5)	1.418(2)	1.417(6)
C6–N2	1.415(4)	1.415(4)	1.387(2)	1.396(5)
N1–C1	1.355(4)	1.349(4)	1.368(2)	1.372(6)
C1–C2	1.369(4)	1.379(5)	1.363(2)	1.355(7)
C2–C3	1.401(5)	1.393(5)	1.412(3)	1.412(6)
C3–C4	1.374(5)	1.373(5)	1.359(2)	1.356(7)
C4–C5	1.407(4)	1.406(4)	1.427(2)	1.421(5)

Thus, the C6–N2 bond lengths in **C2/3b** are shorter than in complexes **A/B**, which is suggestive of stronger “imine” charac-

Table 3. Selected bond lengths [Å] and angles [°] of X-ray crystal structures of complexes **A**,^[15b] **C2**^[15c] and **3b**.

	A	C2	3b
M1–N1	2.094(3)	2.054(3)	2.0711(14)
M1–N2	2.032(2)	2.022(3)	2.0340(14)
M1–Ct1	2.010(3)	1.987(8)	2.0031(13)
M1–Ct2	1.997(3)	1.953(9)	2.0016(12)
M1–Rh2	3.4093(4)	2.8773(3)	2.91468(19)
C8–C9	1.394(4)	1.419(5)	1.403(3)
C12–C13	1.401(5)	1.421(5)	1.403(3)
N1–C5	1.373(3)	1.394(5)	1.385(2)
N1–C1	1.355(4)	1.372(6)	1.368(2)
C1–C2	1.369(4)	1.355(7)	1.363(2)
C2–C3	1.401(5)	1.412(6)	1.412(3)
C3–C4	1.374(5)	1.356(7)	1.359(2)
C4–C5	1.407(4)	1.421(5)	1.427(2)
C5–C6	1.435(4)	1.417(6)	1.418(2)
C6–N2	1.415(4)	1.396(5)	1.387(2)
Rh2–C5	2.925(3)	2.381(4)	2.4696(16)
Rh2–C6	2.130(3)	2.136(4)	2.1356(16)
Rh2–N2	2.254(2)	2.384(3)	2.2246(14)
Rh2–Ct3	2.043(3)	2.027	2.0259(14)
Rh2–Ct4	1.964(3)	2.001	2.0004(13)
C16–C17	1.396(4)	1.388(5)	1.391(3)
C20–C21	1.427(4)	1.408(5)	1.397(3)
N1–M1–Ct1	173.6(1)	174.25	170.61(6)
N2–M1–Ct2	175.7(1)	175.86	175.65(6)
N1–M1–N2	80.4(1)	79.60	79.73(5)
Ct1–M1–Ct2	87.7(1)	86.93	87.77(5)
Ct4–Rh2–M1	108.72	171.17	159.52(4)
Ct3–Rh2–Ct4	87.1(1)	88.32	87.87(6)
M1–C6–Rh2	83.71	68.01	68.87(4)

ter in the former complexes; this is in agreement with the chemical shift differences of the HC=N signals in the ¹H and ¹³C NMR spectra. The C5–C6 bond is also slightly shorter in **3b/C2** than in **A/B**, perhaps indicating pseudo-double-bond character. The distance between N1 and C5 is slightly longer in **3b/C2** than in **A/B**, and the pyridine shows a more distinctive C–C and C=C bond alteration (see Table 2). It is difficult to draw solid conclusions from the C6–N2 and C5–C6 bonds concerning the ligand oxidation states in the complexes because π -coordination of the ligand to the Rh2 centre has an intrinsic elongating effect on these bonds. Previous studies showed that (in contrast to the C6–N2 and C5–C6 bonds) the intraligand bond lengths within the pyridine ring are diagnostic for the ligand oxidation state of dinuclear π -coordinated (reduced) α -imine-pyridine ligand types such as Me-pma-2H.^[15c] As such, these bond lengths are quite similar to those in complex **C2**, in between those expected for the fully neutral and dianionic ligands, but closer to the dianionic form than to the neutral form. Hence, the pyridine bond lengths in the molecular structure of **3b** are diagnostic for the presence of a (Me-pma-2H)²⁻ ligand with a “dearomatised” pyridine ring, rather than a (Me-pma-2H)⁰ ligand. The Rh1–N1 bond length is shorter in **3b** [2.0711(14) Å] than in **A/B** [2.094(3)/2.082(2) Å], which is consistent with a higher degree of charge transfer (delocalisation) into the pyridine moiety.

The coordination mode of **3b** is somewhat similar but not identical to that observed for rhodium in [(cod)Rh^I{(bpa-2H)⁻²}Ir^I(cod)}] complex **C2**. In that case the Rh2 is also assigned to be in the +I oxidation state and the bpa-2H ligand bears the

negative charge. However, the Rh2 centre in **C2** is best described to coordinate to the "iridazabutenyl" moiety, and Rh2 has a somewhat stronger interaction with the C5=C6 bond than with the N2=C6 bond. The Rh2 centre in complex **3b**, on the other hand, seems to interact primarily with the N2-C6-C5 "aza-allyl" moiety, and has a stronger interaction with the N2=C6 bond than with the C5=C6 bond. Furthermore, the Rh2-Rh1 distance in **3b** [2.91468(19) Å] is significantly longer than the Rh2-Ir1 distance in **C2** [2.8773(3) Å]. Hence, the N2-C6-C5 moiety in **3b** is best viewed as an aza-allyl ligand bound to Rh2, with the distance between the aza-allyl centroid Ct and Rh2 being 2.034(1) Å.^[22] In this description, the geometry of the Rh2 in **3b** is, in fact, somewhere between a "tetrahedral" and "square planar" coordination geometry. This distorted geometry may well contribute to a lower cod rotation barrier, in agreement with the ¹H NMR spectroscopic data showing that cod(2) shows fluxional behaviour due to rotation around Rh2, whereas cod(1) is frozen on the NMR timescale. This distorted geometry also corresponds to partial charge transfer from the ligand to Rh2. Nevertheless, taking these observations together, we conclude that Rh2 is best described as being in the +1 oxidation state, adopting a distorted square-planar coordination geometry in its interactions with Rh1, cod(2) and the N2-C6-C5 aza-allyl moiety of the (Me-pma-2H)²⁻ ligand.^[23]

Hence, in contrast to the observations for complex **A**, the structural parameters and NMR spectroscopic observations for **3b** suggest limited electron-transfer from the doubly deprotonated (Me-pma-2H)²⁻ ligand to Rh2. Instead, electron delocalization into the pyridine moiety occurs with extensive "dearomatization" of the pyridine moiety, which still leads to a substantial "imine" character of the N2=C6 moiety. The reluctance of Rh2 to undergo formal reduction from rhodium(+1) to rhodium(-1) in complex **3b** is presumably due to the absence of an additional pyridine donor in close proximity [which stabilises the respective rhodium(-1) centre, because a tetrahedral geometry similar to that observed in complex **A** is no longer accessible]. It should be noted that exogenous donors, such as a free pma ligand, do not seem to readily coordinate to the Rh2 centre to induce ligand-to-metal charge transfer (see Scheme 6). The coordination mode observed for **3b** is complementary to the coordination modes **I** previously observed for complexes **A**, **B** and **C1** and coordination mode **II** observed for complex **C2** (Figure 4).

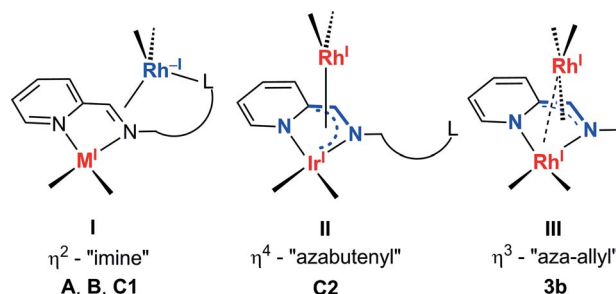


Figure 4. Three geometric and electronic structures of the bimetallic Rh or Ir complexes featuring a doubly deprotonated ditopic picolyl-amine ligand.

The versatility of the Rh2 coordination mode reflects the rich interplay between the metal and ligand, and demonstrates a

variety of electron-transfer and charge-delocalisation processes from the doubly deprotonated C6-N2 moiety, which results in a continuum for the diamide-to-picolylimine redox chemistry.

Synthesis of the Bimetallic Complex **3a**

The iridium analogue of **3b**, [(cod)Ir^I{(Me-pma-2H)²⁻}Ir^I(cod)] (**3a**), was also synthesised and was isolated as a deep brownish-red solid. The complex was prepared by reacting [(Ir(cod)(μ-OMe))₂] with two equivalents of the Me-pma ligand in Et₂O. Suitable crystals of **3a** could not be obtained, and we therefore turned to DFT calculations to elucidate the preferred geometry. We first validated our computational approach by comparing the DFT optimised geometry of [(cod)Rh^I{(Me-pma-2H)²⁻}Rh^I(cod)] (**3b'**) (bp86/def2-TZVPP level employing Grimme's D3 dispersion corrections) with the structure of **3b** determined by X-ray diffraction (see Table S1 in the Supporting Information). The structure of [(cod)Ir^I{(Me-pma-2H)²⁻}Ir^I(cod)] (**3a'**) was computed at the same level of theory to serve as a model for **3a**. The geometry of **3a'** is analogous to that of **3b**, with the Ir1(cod) fragment coordinated to the Me-pma-2H ligand plane and the Ir2(cod) fragment seemingly interacting with the N2-C6-C5 "aza-allyl" moiety. Ir2 is again best described as an iridium(+1) centre and there is once more substantial charge delocalisation over the pyridine ring, as can be seen from the partial dearomatization of the ring indicated by the alternating bond C-C lengths. Complexes **3a'** and **3b/3b'** are very similar, except for the substantially longer N2=C6 distance in **3a'**, which indicates that the N2=C6 moiety has a somewhat smaller "imine" character in **3a'**. As observed for Rh2 in **3b/3b'**, Atom Ir2 likely interacts slightly stronger with N2=C6 in **3a'** than in **3b'**, given the slightly longer bond length for M2-C5 (Δ = 0.078 Å) and M2-N2 (Δ = 0.019 Å), and the larger C5-C6-M2 angle (Δ = 2.99°) and N2-C6-M2 (Δ = 1.27°). Overall, the geometric and electronic structure of **3a'** is similar to those of **3b/3b'**.

Catalytic Activity of **1a** and **1b** in Ketene Formation by Carbonylation of Carbenes

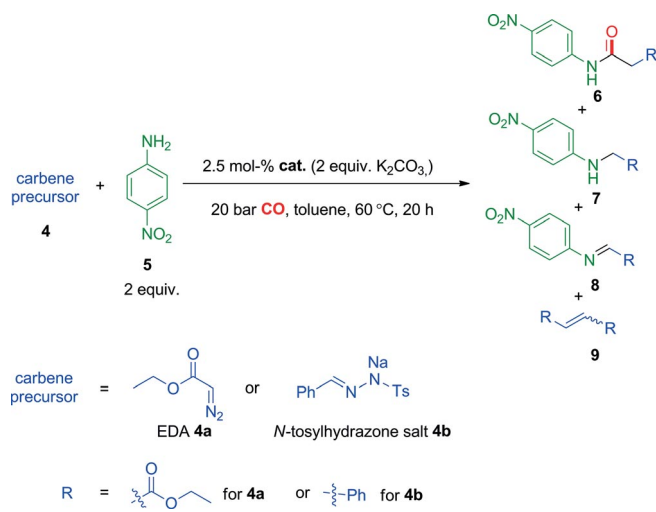
Ketenes are highly active and very useful intermediates for the synthesis of a wide range of chemicals.^[24] Although carbonylation of transition-metal carbenes is a promising synthetic method to produce ketenes,^[25] providing a valuable alternative to conventional methods that have clear limitations,^[26] most systems developed to date involve only stoichiometric reactions.^[27] Catalytic ketene formation by using cobalt and palladium^[28] catalysts was reported recently. A variety of esters, amides and β-lactams were accessible via the ketene intermediates that were generated in situ.

However, whereas chiral induction in these coupling reactions is highly desirable,^[29] none of the reported catalysts is capable of both catalysing ketene formation from carbene and promoting the following coupling reactions in an enantioselective manner [e.g., when several chiral Co(porphyrin) complexes were used as catalysts, no *ee* was detected^[28e]]. This is attributed to the relatively low affinity of these metal centres to bind the ketene intermediates. We reasoned that complexes **1a** and

1b might serve as suitable catalyst candidates for this purpose. Rhodium complexes are known to promote stoichiometric ketene formation by carbonylation of carbenes,^[30] and rhodium complexes should display a relatively strong affinity to bind the resulting ketenes. With suitable metal complexes, this might eventually lead to the development of enantioselective catalytic protocols. We recently reported on the activity of rhodium complexes with PNN pincer-type ligands in catalytic carbene carbonylation reactions,^[18] showing that rhodium is indeed a good candidate for further developments in this field. Therefore, we wondered whether rhodium(I) complexes with bidentate N-donor ligands could also facilitate this reaction, because these ligands may be more easily modified to tune (enantio)selectivity in future studies. Iridium might also be a good candidate, because it can be expected to bind ketenes even more strongly, even though Ir complexes are thus far less explored as mediators for ketene formation reactions.

The reactions were performed by using previously reported conditions of 20 bar CO at 60 °C (Table 4).^[18,28e,28f] Ethyl diazoacetate (EDA) **4a** and sodium 2-benzylidene-1-tosylhydrazin-1-ide (**4b**) were tested as carbene precursors, and 4-nitroaniline was used as the nucleophile to trap the ketene intermediates to form amide product **6**. By using **1b** as catalyst, the corresponding amide products were obtained in 78 and 62 % yield with **4a** and **4b**, respectively, with base being employed for **4a**. The yields are similar to those obtained with Co,^[28e] Pd^[28f] and Rh^[18] systems. The reactions generally yielded a mixture of products that was analysed by NMR spectroscopy and GC-MS.

Table 4. Catalytic carbene carbonylation reactions studied by using catalyst precursors **1a** and **1b**, carbene precursors **4a** and **4b**, and 4-nitroaniline **5** as the ketene trapping agent. Besides the desired products **6a** and **6b**, side products **7-9** are also formed.



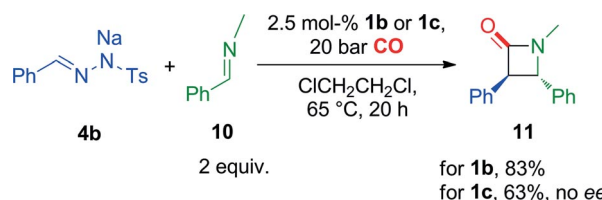
Entry	4	Catalyst	K ₂ CO ₃	6	7	8	9
1	4a	1a	no	3	32	0	9
2	4a	1a	yes	0	14	0	0
3	4a	1b	no	11	31	0	18
4	4a	1b	yes	78	20	0	0
5 ^[a]	4b	1a	no	0	0	0	0
6	4b	1b	no	62	0	19	0

[a] Unidentified side products formed.

For substrate **4a**, the amine side product **7a**, arising from direct coupling between metalcarbene and 4-nitroaniline **5**, was always formed in a significant amount, along with the alkene side product **9a** formed from dimerisation of the carbene. Addition of K₂CO₃ reduced the formation of **7a** and **9a** (Table 4, entries 1–4). For the iridium precatalyst **1a**, monodeprotonation of the Me-pma ligand would lead to a more electron-rich amido complex with concomitantly enhanced π -back donation from the metal to the carbene *p*-orbital. This would reduce the electrophilicity of the carbene, thus suppressing its propensity for coupling with 4-nitroaniline and carbene dimerisation through coupling with the carbene precursor. For rhodium precatalyst **1b**, the exact form of the active metal complex is less clear, because deprotonation of the Me-pma ligand of **1b** can lead to formation of dinuclear complex **3b** (see above). Whether or not such a disproportionation reaction also occurs under (diluted) catalytic conditions is not clear.

Iridium complex **1a** showed poor activity and selectivity with respect to product **6** with both carbene precursors **4a** and **4b** (Table 4, entries 1, 2 and 5). The rhodium precatalyst **1b** showed good activity and selectivity to produce **6** from both **4a** and **4b** under basic conditions (entries 4 and 6; note that **4b** is also a moderately strong base, so both **1a** and **1b** should be in their deprotonated forms when using an excess of this substrate). Surprisingly, when **4b** was used as the carbene precursor, imine side product **8b** was observed and the corresponding amine side product **7b** was not detected.^[31] The iridium complex **1a** clearly has a lower activity than rhodium complex **1b** in catalytic ketene formation.

β -Lactams are medicinally important structures and versatile building blocks for the construction of other valuable compounds.^[32] A widely applied β -lactam synthetic method is the [2+2] Staudinger reaction between a ketene and an imine.^[33] Interestingly, complex **1b** can also be used to catalyse the formation of β -lactams from an in situ generated ketene (using **4b**) and imine **10** in a one-pot synthetic protocol by using similar conditions to those reported previously (Scheme 7).^[18,28e,28f] Complex **1a** shows good activity in this reaction, producing β -lactam **11** in 83 % yield, with the *trans*-configured product being detected exclusively.^[34] The yield is similar to that of the reported Pd^[28f] system but higher than those of the Co^[28e] and Rh systems.^[18] Furthermore, the obtained *trans*-stereoselectivity is higher than observed with either the Co^[28e] or Pd^[28f] system.



Scheme 7. β -Lactam **11** synthesis through ketene formation from **4b** catalysed by catalyst precursors **1a** and **1c**.

Given that methods for enantioselective β -lactam synthesis are highly desirable,^[35] we were prompted to synthesise a chiral analogue of **1b** for enantioselective catalysis. For this purpose, we synthesised chiral complex **1c** (Figure 5). Complex **1c** was prepared by using Bn*-pma ligand [(*R*)-1-phenyl-*N*-(pyridin-2-

ylmethyl)ethanamine], bearing a chiral benzylethyl auxiliary instead of a methyl group in pma. The cation in complex **1c** adopts an almost identical square-planar geometry around rhodium as **1b** (Figure 5), with only slightly longer Rh–N2 [$\Delta = 0.0301(16)$ Å] and similar Rh–N1 [$\Delta = -0.0043(17)$ Å] bonds. The decreased orbital overlap due to the steric bulk of the benzylethyl group at N2 results in a larger (\angle N2–Rh–Ct1 angle of $98.25(4)^\circ$ in **1c** (vs. $95.66(5)^\circ$ in **1b**). Complex **1c** also showed good catalytic activity to produce β -lactam **11** with a yield of 63%. Unfortunately, no *ee* was detected for this reaction. This could have several reasons: (i) Premature dissociation of the ketene fragment from the catalyst could be the problem, (ii) (partial) Bn^* -pma ligand dissociation could occur, or (iii) the chiral moiety is simply too remote from the coordinated ketene for efficient chirality transfer. Further studies on this process are in progress to unravel the detailed mechanism and prospects for chirality transfer with related catalysts.

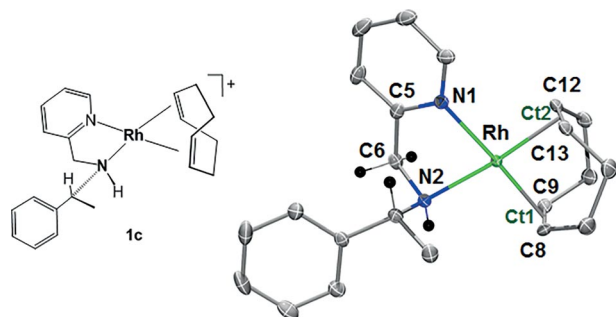


Figure 5. Left: Line drawing of the cation of chiral complex **1c**. Right: Molecular structure (ORTEP at 50% level) of the cation of complex **1c**. Hydrogen atoms are removed for clarity, except for those on C6, N2 and C7. Selected bond lengths [Å] and angles [°]: Rh–N1, 2.0922(12); Rh–N2, 2.1448(10); Rh–Ct1, 2.0285(11); Rh–Ct2, 2.0145(9); N1–C5, 1.3586(17); C5–C6, 1.505(2); C6–N2, 1.500(2); N2–C7, 1.5073(17); C15–C16, 1.3879(19); C19–C20, 1.395(2); N1–Rh–Ct1, 172.12(4); N2–Rh–Ct2, 174.21(4); N1–Rh–N2, 77.60(4); Ct1–Rh–Ct2, 87.47(4); Rh–N2–C6, 101.51(9); Ct1–Ct2–N2–C7, 110.82(9)°.

Conclusions

Rhodium and iridium(cod) cationic complexes **1a** and **1b** based on Me-pma ligand were synthesised. Upon reaction with one equivalent KOtBu , **1a** gives rise to quantitative formation of the neutral amido $[\text{Ir}(\text{cod})(\text{Me-pma-H})]$ complex **2a**, whereas **1b** leads to the formation of a dinuclear rhodium complex **3b** featuring a doubly deprotonated Me-pma-2H ditopic ligand. NMR spectroscopy and X-ray crystal structure determination confirm that there is negligible ligand-to-metal charge-transfer from the doubly deprotonated Me-pma ligand to Rh2. The negative charge remains on the (pma-2H)²⁻ fragment, but substantial charge delocalization into the pyridine ring occurs leading to partial pyridine “dearomatisation”. The geometry of the corresponding dinuclear iridium complex **3a** is similar to that of **3b**, according to DFT studies. The collected data support the previous assumption that coordination of an additional ligand donor to M2 is necessary to induce formal reduction of M(+I) to M(–I) through electron transfer of the dianionic π -coordinated “1,2-diyldiamide” (N–Py–C=C–N-amido) moiety of the ligand to M2 to form a neutral imine (NPy–C–C=N–) ligand moiety, wherein

the additional ligand donor is proposed to stabilise the corresponding reduced d¹⁰ M(–I) ion in a tetrahedral geometry. The X-ray crystal structure of **3b** and the DFT optimised geometry of **3a** further disclose an “aza-allyl” η^3 -coordination mode of the (Me-pma-2H)²⁻ ligand bound to M2. The observations described in this paper, combined with the previously reported results, demonstrate a series of intermediate states of metal-bound picolyl-amines after double deprotonation. The electron-transfer and charge-delocalisation processes are sensitive to a number of factors, such as the nature of the sigma-bound metal (M1), the nature of the π -coordinated metal M2 acting as a potential “oxidant”, and the presence or absence of an additional pendant coordinating ligand donor which can stabilise a tetrahedral M(–I) ion.

The activity of Ir complex **1a** and Rh complex **1b** in catalytic carbene carbonylation reactions was evaluated. Rhodium complex **1c**, a chiral analogue of **1b**, was also used for this purpose. Rhodium complex **1b** showed much better catalytic activity for ketene formation from diazo-derived carbenes than Ir complex **1a**, with amides and β -lactams synthesised in good yields via the intermediacy of metal-bound carbenes. Chiral complex **1c** has an activity similar to that of **1b**, but no chirality transfer was observed in initial attempts to achieve enantioselective one-pot synthesis of β -lactams from a carbene precursor, CO and an imine. Mechanistic studies to elucidate the catalytic process and to progress catalyst development towards enantioselective catalysis in ketene chemistry are ongoing in our group.

Experimental Section

General: All the reactions were carried out under argon using standard Schlenk techniques. Metal precursors $[\{\text{M}(\text{cod})(\mu\text{-Cl})\}_2]$ ^[36] and $[\{\text{M}(\text{cod})(\mu\text{-OMe})\}_2]$ ^[37] as well as complexes **1**,^[38] **2b**^[15b] and **3**^[15b] were synthesised according to known procedures. The Me-pma ligand was obtained from Aldrich and used as received. NMR spectroscopic measurements were recorded with a Bruker AV 400 spectrometer. Chemical shifts are reported and referenced to SiMe_4 , using the internal signal of deuterated solvent as reference. HRMS were obtained with a time-of-flight JEOL AccuTOF LC-plus mass spectrometer (JMS-T100LP). Elemental analyses were carried out by Kolbe Mikroanalytisches Labor (Mülheim/Ruhr, Germany).

In situ Ketene Synthesis from Carbene Carbonylation for Coupling: In a typical carbonylation experiment a stainless steel autoclave (150 mL) suitable for seven reaction vessels (equipped with Teflon mini stirring bars) was used to perform parallel reactions. Each vial was charged with carbene precursor (EDA **4a** or *N*-tosyl-hydrazone sodium salt **4b**, 0.15 mmol), amine nucleophile **5** or imine **10** (0.30 mmol), catalyst (0.0075 mmol), internal standard 1,3,5-trimethoxybenzene (0.015 mmol) and solvent (3 mL). Before starting the catalytic reactions, the charged autoclave was purged (5 \times) with 20 bar CO and then pressurised to the desired pressure. The autoclave was heated in an oil-bath with the vials being stirred overnight. After the reaction time, the autoclave was cooled to 0 °C and vented to 1 atm. Around 1.5 mL of each reaction mixture was taken out, the solvent was removed by using rotary evaporation, the residue was dissolved in CDCl_3 or CH_2Cl_2 (and filtered when necessary) for ¹H NMR and GC–MS analysis, respectively. The conversion and yield for each reaction were calculated based on the integration of ¹H NMR signals of corresponding species relative to

that of the internal standard (1,3,5-trimethoxybenzene). Product assignment followed reported assignments.^[28e,28f]

Complex 1a: The ligand Me-pma (93.8 μL , 0.763 mmol, 2.05 equiv.) was added to a solution of $[\{\text{Ir}(\text{cod})(\mu\text{-O}Me)\}_2]$ (250.0 mg, 0.372 mmol, 1 equiv.) in methanol (10 mL), followed by addition of NH_4PF_6 (121.3 mg, 0.744 mmol, 2 equiv.). The solution was stirred for 1 h and then concentrated to 5 mL under vacuum. The yellow precipitate was collected by filtration and washed with a small amount of cold methanol and dried in vacuo, yield 367.8 mg (87 %). ^1H NMR (400 MHz, CD_2Cl_2): δ = 8.09–8.01 (m, 2 H, Py), 7.74 (d, J = 7.9 Hz, 1 H, Py), 7.49 (ddd, J = 7.4, 5.7, 1.4 Hz, 1 H, Py), 4.71–4.57 (m, 2 H, Py- CH_2N , NH), 4.25–4.12 (m, 3 H, Py- CH_2N , cod-vinyl), 4.11–4.02 (m, 2 H, cod-vinyl), 2.67 (d, J = 5.9 Hz, 3 H, CH_3), 2.46–2.19 (m, 4 H, cod-allyl), 2.05–1.87 (m, 2 H, cod-allyl), 1.87–1.59 (m, 2 H, cod-allyl) ppm. $^{13}\text{C}\{^1\text{H}\}$ NMR (100 MHz, CD_2Cl_2): δ = 163.39 (C_{Py}), 148.15 (C_{Py}), 141.46 (C_{Py}), 125.33 (C_{Py}), 123.23 (C_{Py}), 70.69 ($\text{C}_{\text{cod-vinyl}}$), 69.05 ($\text{C}_{\text{cod-vinyl}}$), 68.36 ($\text{C}_{\text{cod-vinyl}}$), 67.72 ($\text{C}_{\text{cod-vinyl}}$), 62.10 (Py- CH_2N), 40.05 (CH_3), 32.40 ($\text{C}_{\text{cod-allyl}}$), 31.22 ($\text{C}_{\text{cod-allyl}}$), 31.09 ($\text{C}_{\text{cod-allyl}}$), 30.09 ($\text{C}_{\text{cod-allyl}}$) ppm. HRMS (ESI, 243 K, CH_2Cl_2): m/z calcd. for $[\text{M}]^+$ 423.1407; found 423.1498. $\text{C}_{15}\text{H}_{22}\text{F}_6\text{IrN}_2\text{P}$ (567.5): calcd. C 31.74, H 3.91, N 4.94; found C 31.66, H 3.94, N 4.96.

Complex 1b: Synthesised as described for **1a**, yield 81 %. ^1H NMR (400 MHz, CD_2Cl_2): δ = 7.94 (td, J = 7.7, 1.5 Hz, 1 H, Py), 7.72 (dd, J = 5.7, 1.3 Hz, 1 H, Py), 7.56 (d, J = 7.9, 1.2 Hz, 1 H, Py), 7.41 (ddd, J = 7.2, 5.6, 1.3 Hz, 1 H, Py), 4.59–4.42 (m, 2 H, Py- CH_2N , cod-vinyl), 4.39–4.18 (m, 3 H, cod-vinyl), 3.99 (dd, J = 15.9, 5.9 Hz, 1 H, Py- CH_2N), 3.82–3.70 (br., 1 H, NH), 2.66–2.37 (m, 4 H, cod-allyl), 2.51 (d, J = 6.2 Hz, 3 H, CH_3), 2.17–1.87 (m, 4 H, cod-allyl) ppm. $^{13}\text{C}\{^1\text{H}\}$ NMR (100 MHz, CD_2Cl_2): δ = 161.60 (C_{Py}), 147.88 (C_{Py}), 140.59 (C_{Py}), 124.78 (C_{Py}), 123.35 (C_{Py}), 85.03 (d, J = 12.4 Hz, $\text{C}_{\text{cod-vinyl}}$), 83.79 (d, J = 12.7 Hz, $\text{C}_{\text{cod-vinyl}}$), 83.69 (d, J = 6.2 Hz, $\text{C}_{\text{cod-vinyl}}$), 83.57 (d, J = 5.8 Hz, $\text{C}_{\text{cod-vinyl}}$), 60.83 (Py- CH_2N), 39.16 (CH_3), 31.45 ($\text{C}_{\text{cod-allyl}}$), 30.57 ($\text{C}_{\text{cod-allyl}}$), 31.46 ($\text{C}_{\text{cod-allyl}}$), 29.79 ($\text{C}_{\text{cod-allyl}}$) ppm. HRMS (ESI, 243 K, CH_2Cl_2): m/z calcd. for $[\text{M}]^+$ 333.0833; found 333.0865. $\text{C}_{15}\text{H}_{22}\text{F}_6\text{N}_2\text{PRh}$ (478.2): calcd. C 37.67, H 4.64, N 5.86; found C 37.08, H 4.63, N 5.72.

Complex 2a. Method I: Potassium *tert*-butoxide (KOtBu, 3.3 mg, 29.1 μmol , 1.1 equiv.) was added to a yellow solution of **1a** (15.0 mg, 26.4 μmol , 1 equiv.) in $[\text{D}_8]\text{THF}$ (0.6 mL) in a Schlenk vessel whilst stirring, which resulted in an immediately colour change to deep-red. The solution was transferred to a sealed NMR tube and directly analysed by NMR spectroscopy.

Method II: The ligand Me-pma (51.4 μL , 0.418 mmol, 1 equiv.) was added to a yellow suspension of $[\{\text{Ir}(\text{cod})(\mu\text{-O}Me)\}_2]$ (278 mg, 0.418 mmol, 1 equiv.) in diethyl ether (14 mL), which resulted in a colour change to deep-red. After stirring for 20 min, the solvent was concentrated to around 8 mL by evaporation under vacuum, layered with 15 mL of pentane and stored at -4°C overnight. The mother liquor was decanted and the solid was washed with pentane and dried in vacuo. ^1H NMR (400 MHz, $[\text{D}_8]\text{THF}$): δ = 8.01 (d, J = 5.9 Hz, 1 H, Py), 7.78 (dd, J = 7.8, 1.5 Hz, 1 H, Py), 7.65 (d, J = 7.6 Hz, 1 H, Py), 7.19 (ddd, J = 7.6, 6.2, 1.3 Hz, 1 H, Py), 4.57 (s, 2 H, Py- CH_2N), 3.74–3.69 (m, 2 H, cod-vinyl), 2.93 (s, 3 H, CH_3), 2.71–2.65 (m, 2 H, cod-vinyl), 2.26–2.12 (m, 4 H, cod-allyl), 1.75–1.61 (m, 4 H, cod-allyl) ppm. $^{13}\text{C}\{^1\text{H}\}$ NMR (100 MHz, CD_2Cl_2): δ = 172.04 (C_{Py}), 146.45 (C_{Py}), 136.78 (C_{Py}), 122.67 (C_{Py}), 120.73 (C_{Py}), 73.49 (Py- CH_2N), 63.01 ($\text{C}_{\text{cod-vinyl}}$), 53.31 ($\text{C}_{\text{cod-vinyl}}$), 42.01 (CH_3), 33.26 ($\text{C}_{\text{cod-allyl}}$), 32.52 ($\text{C}_{\text{cod-allyl}}$) ppm. HRMS (ESI, 243 K, THF): m/z calcd. for $[\text{M}]^+$ 423.1407; found 423.1406.

Complex 3a: The ligand Me-pma ligand (51.4 μL , 0.418 mmol, 1 equiv.) was added to a yellow suspension of $[\{\text{cod}\}\text{Ir}(\mu\text{-O}Me)_2]$

(278 mg, 0.418 mmol, 1 equiv.) in diethyl ether (14 mL), giving a deep-red colour. After stirring for 20 min, the solvent was concentrated to around 8 mL by evaporation under vacuum, layered with 15 mL of pentane and stored at -4°C overnight. The mother liquor was decanted and the solid was washed with pentane and dried. ^1H NMR (400 MHz, C_6D_6): δ = 7.72 (dt, J = 5.9, 1.1 Hz, 1 H, Py), 6.66 (dd, J = 7.6, 1.5 Hz, 1 H, Py), 6.61 (d, J = 7.4 Hz, 1 H, py), 6.14 (tm, J = 7.5 Hz, 1 H, Py), 4.34 (s, 2 H, cod-vinyl), 3.58–3.52 (m, 2 H, cod-vinyl), 3.19 (s, 3 H, CH_3), 3.02 (s, 1 H, Py- $\text{CH}=\text{N}$), 2.95 (br., 2 H, cod-allyl), 2.53 (br., 4 H, cod-allyl), 2.21–2.08 (m, 4 H, cod-allyl), 1.99 (d, J = 8.0 Hz, 4 H, cod-allyl), 1.41–1.28 (m, 4 H, cod-allyl) ppm. $^{13}\text{C}\{^1\text{H}\}$ NMR (100 MHz, C_6D_6): δ = 170.95 (C_{Py}), 145.63 (C_{Py}), 135.16 (C_{Py}), 121.52 (C_{Py}), 119.78 (C_{Py}), 89.82 (Py- $\text{CH}=\text{N}$), 64.52 ($\text{C}_{\text{cod-vinyl}}$), 59.09 ($\text{C}_{\text{cod-vinyl}}$), 58.59 ($\text{C}_{\text{cod-vinyl}}$), 57.18 ($\text{C}_{\text{cod-vinyl}}$), 54.14 ($\text{C}_{\text{cod-vinyl}}$), 42.11 (CH_3), 36.23 ($\text{C}_{\text{cod-allyl}}$), 34.58 ($\text{C}_{\text{cod-allyl}}$), 33.97 ($\text{C}_{\text{cod-allyl}}$), 32.83 ($\text{C}_{\text{cod-allyl}}$), 32.69 ($\text{C}_{\text{cod-allyl}}$), 31.87 ($\text{C}_{\text{cod-allyl}}$) ppm. Correct mass data could not be obtained possibly due to the instability of the complex under the applied conditions.

Complex 3b: The ligand Me-pma (63.4 μL , 0.516 mmol, 1 equiv.) was added to a suspension of $[\{\text{Rh}(\text{cod})(\mu\text{-O}Me)\}_2]$ (250 mg, 0.615 mmol, 1 equiv.) in diethyl ether (15 mL). The colour changed to orange and then to deep red. After stirring for 20 min, the solvent was concentrated to around 5 mL by evaporation under vacuum, layered with 10 mL of pentane and stored in the fridge (-4°C) overnight. The mother liquor was decanted and the solid was washed with pentane and dried under vacuum, yield 172.8 mg (62 %). ^1H NMR (400 MHz, C_6D_6): δ = 6.56 (dd, J = 6.5, 1.2 Hz, 1 H, py), 6.47 (ddd, J = 8.9, 6.4, 1.4 Hz, 1 H, py), 6.16 (dt, J = 8.8, 1.2 Hz, 1 H, py), 5.68 (td, J = 6.4, 1.4 Hz, 1 H, py), 5.16 (dd, J = 0.8, 0.8 Hz, 1 H, Py- $\text{CH}=\text{N}$), 4.98–3.76 (br., 5 H, cod-vinyl), 4.27–4.19 (m, 1 H, cod-vinyl), 3.74–3.63 (m, 2 H, cod-vinyl), 3.47–3.38 (m, 1 H, cod-vinyl), 2.78–2.66 (m, 1 H, cod-allyl), 2.65–2.54 (m, 1 H, cod-allyl), 2.58 (t, J = 1.1 Hz, 3 H, CH_3), 2.38–2.19 (m, 5 H, cod-allyl), 2.19–2.10 (m, 1 H, cod-allyl), 2.05–1.92 (m, 4 H, cod-allyl), 1.85–1.71 (m, 4 H, cod-allyl) ppm. $^{13}\text{C}\{^1\text{H}\}$ NMR (100 MHz, C_6D_6): δ = 141.99 (C_{Py}), 130.93 (d, J = 1.6 Hz, C_{Py}), 128.24 (C_{Py}), 114.54 (C_{Py}), 108.03 (C_{Py}), 89.78 (d, J = 5.5 Hz, Py- $\text{CH}=\text{N}$), 77.78 (d, J = 13.4 Hz, $\text{C}_{\text{cod-vinyl}}$), 75.80 (d, J = 12.8 Hz, $\text{C}_{\text{cod-vinyl}}$), 74.26 (d, J = 12.2 Hz, $\text{C}_{\text{cod-vinyl}}$), 72.06 (d, J = 12.5 Hz, $\text{C}_{\text{cod-vinyl}}$), 43.12 (d, J = 1.7 Hz, CH_3), 33.58 ($\text{C}_{\text{cod-allyl}}$), 32.06 ($\text{C}_{\text{cod-allyl}}$), 31.30 ($\text{C}_{\text{cod-allyl}}$), 30.14 ($\text{C}_{\text{cod-allyl}}$), 29.15 ($\text{C}_{\text{cod-allyl}}$) ppm. HRMS (ESI, 243 K, C_6D_6): m/z calcd. for $[\text{M}-\text{H}]^+$ 541.0592; found 541.0626.

Complex 1c: Synthesised as described for **1a**, yield 56 %. Surprisingly, complex **1c** is in equilibrium with another unidentified species with a ratio of ca. 1:0.6 in CD_2Cl_2 (Figure S20,21), whereas addition of half the volume of CD_3CN resulted in the sole existence of **1c**. ^1H NMR (400 MHz, CD_2Cl_2 , 1/2 CD_3CN): δ = 7.84 (td, J = 7.8, 1.5 Hz, 1 H, H_{Py}), 7.57 (d, J = 5.6 Hz, 1 H, H_{Py}), 7.47–7.38 (m, 1 H, 2 H, H_{Py} , H_{Ph}), 7.34–7.22 (m, 1 H, 3 H, H_{Py} , H_{Ph}), 4.25 (br., 4 H, $\text{H}_{\text{cod-vinyl}}$), 4.16–3.89 (br., 1 H, 2 H, NH, Py- $\text{CH}=\text{N}$), 3.67 [q, J = 7.0 Hz, 1 H, $\text{NCH}(\text{Me})\text{Ph}$], 2.43 (ddt, J = 14.0, 9.8, 6.9 Hz, 2 H, $\text{H}_{\text{cod-allyl}}$), 2.27 (br., 2 H, $\text{H}_{\text{cod-allyl}}$), 1.94 (br., 2 H, $\text{H}_{\text{cod-allyl}}$), 1.812.27 (br., 2 H, $\text{H}_{\text{cod-allyl}}$), 1.61 (d, J = 6.9 Hz, 3 H, Me) ppm. $^{13}\text{C}\{^1\text{H}\}$ NMR (100 MHz, CD_2Cl_2 , 1/2 CD_3CN): δ = 162.01 (C_{Py}), 147.75 (C_{Py}), 139.91 (C_{Py}), 139.71 (C_{Ph}), 129.12 (C_{Ph}), 128.99 (C_{Ph}), 127.91 (C_{Ph}), 124.44 (C_{Py}), 123.13 (C_{Py}), 83.42–82.44 (m, $\text{C}_{\text{cod-vinyl}}$), 60.98 (s, PhCHMe), 54.90–54.67 (m, Py- CH_2N), 30.48 ($\text{C}_{\text{cod-allyl}}$), 29.81 ($\text{C}_{\text{cod-allyl}}$), 19.72 (CH_3) ppm. HRMS (ESI, 243 K, CH_2Cl_2): m/z calcd. for $[\text{M}]^+$ 423.1308; found 423.1321.

X-ray Crystal Structure Determination of 1a: $[\text{C}_{15}\text{H}_{22}\text{IrN}_2](\text{PF}_6)$; 567.52; dark-yellow block; $0.49 \times 0.46 \times 0.33 \text{ mm}^3$; monoclinic; $P2_1/c$ (no. 14); $a = 6.4624(2)$, $b = 15.9677(4)$, $c = 17.1755(4) \text{ \AA}$, $\beta =$

101.2505(10) $^\circ$; $V = 1738.28(8) \text{ \AA}^3$; $Z = 4$; $D_x = 2.169 \text{ g/cm}^3$; $\mu = 7.83 \text{ mm}^{-1}$. 25066 Reflections were measured with a Bruker Kappa ApexII diffractometer with sealed tube and Triumph monochromator ($\lambda = 0.71073 \text{ \AA}$) at a temperature of 150(2) K up to a resolution of $(\sin \theta/\lambda)_{\text{max}} = 0.65 \text{ \AA}^{-1}$. The intensities were integrated with the SAINT software.^[39] Multiscan absorption correction and scaling was performed with SADABS^[40] (correction range 0.26–0.43). 4020 Reflections were unique ($R_{\text{int}} = 0.020$), of which 3895 were observed [$I > 2\sigma(I)$]. The structure was solved with Direct Methods using SHELXS-97.^[41] Least-squares refinement was performed with SHELXL-97^[41] against F^2 of all reflections. Non-hydrogen atoms were refined freely with anisotropic displacement parameters. All hydrogen atoms were located in difference Fourier maps. The N–H hydrogen atom and the four C–H hydrogen atoms at the coordinated double bonds were refined freely with isotropic displacement parameters. All other hydrogen atoms were refined with a riding model. 247 Parameters were refined with no restraints. R_1/wR_2 [$I > 2\sigma(I)$]: 0.0146/0.0338. R_1/wR_2 [all reflections]: 0.0154/0.0340, $S = 1.160$. Residual electron density between -0.74 and 0.88 e/\AA^3 . Geometry calculations and checking for higher symmetry was performed with the PLATON program.^[42]

X-ray Crystal Structure Determination of 1b: $[\text{C}_{15}\text{H}_{22}\text{N}_2\text{Rh}](\text{PF}_6)$; 478.23; yellow-green block; $0.30 \times 0.09 \times 0.09 \text{ mm}^3$; monoclinic; $P2_1/c$ (no. 14); $a = 6.5163(2)$, $b = 16.0417(4)$, $c = 17.1102(5) \text{ \AA}$, $\beta = 101.2918(10)^\circ$; $V = 1753.95(9) \text{ \AA}^3$; $Z = 4$; $D_x = 1.811 \text{ g/cm}^3$; $\mu = 1.13 \text{ mm}^{-1}$. 33645 Reflections were measured with a Bruker Kappa ApexII diffractometer with sealed tube and Triumph monochromator ($\lambda = 0.71073 \text{ \AA}$) at a temperature of 150(2) K up to a resolution of $(\sin \theta/\lambda)_{\text{max}} = 0.65 \text{ \AA}^{-1}$. The intensities were integrated with the SAINT software.^[40] Multiscan absorption correction and scaling was performed with SADABS^[40] (correction range 0.67–0.75). 4050 Reflections were unique ($R_{\text{int}} = 0.018$), of which 3772 were observed [$I > 2\sigma(I)$]. The structure was solved with Direct Methods using SHELXS-97.^[41] Least-squares refinement was performed with SHELXL-97^[41] against F^2 of all reflections. Non-hydrogen atoms were refined freely with anisotropic displacement parameters. All hydrogen atoms were located in difference Fourier maps. The N–H hydrogen atom and the four C–H hydrogen atoms at the coordinated double bonds were refined freely with isotropic displacement parameters. All other hydrogen atoms were refined with a riding model. 247 Parameters were refined with no restraints. R_1/wR_2 [$I > 2\sigma(I)$]: 0.0174/0.0436. R_1/wR_2 [all reflections]: 0.0194/0.0446, $S = 1.041$. Residual electron density between -0.34 and 0.66 e/\AA^3 . Geometry calculations and checking for higher symmetry was performed with the PLATON program.^[42]

X-ray Crystal Structure Determination of 2a: $\text{C}_{15}\text{H}_{21}\text{IrN}_2$; 421.54; red block; $0.21 \times 0.17 \times 0.16 \text{ mm}^3$; monoclinic; $P2_1/c$ (no. 14); $a = 9.2085(3)$, $b = 11.6486(3)$, $c = 13.1155(4) \text{ \AA}$, $\beta = 109.281(1)^\circ$; $V = 1327.93(7) \text{ \AA}^3$; $Z = 4$; $D_x = 2.108 \text{ g/cm}^3$; $\mu = 10.04 \text{ mm}^{-1}$. 53739 Reflections were measured with a Bruker Kappa ApexII diffractometer with sealed tube and Triumph monochromator ($\lambda = 0.71073 \text{ \AA}$) at a temperature of 150(2) K up to a resolution of $(\sin \theta/\lambda)_{\text{max}} = 0.65 \text{ \AA}^{-1}$. The intensities were integrated with the Eval15 software.^[43] Multiscan absorption correction and scaling was performed with SADABS^[40] (correction range 0.29–0.44). 5809 Reflections were unique ($R_{\text{int}} = 0.025$), of which 5267 were observed [$I > 2\sigma(I)$]. The structure was solved with automated Patterson methods using DIRDIF-08.^[44] Least-squares refinement was performed with SHELXL-97^[41] against F^2 of all reflections. Non-hydrogen atoms were refined freely with anisotropic displacement parameters. All hydrogen atoms were located in difference Fourier maps. The four C–H hydrogen atoms at the coordinated double bonds were refined freely with isotropic displacement parameters. All other hydrogen

atoms were refined with a riding model. 180 Parameters were refined with no restraints. R_1/wR_2 [$I > 2\sigma(I)$]: 0.0128/0.0260. R_1/wR_2 [all reflections]: 0.0157/0.0265, $S = 1.057$. Residual electron density between -0.88 and 0.73 e/\AA^3 . Geometry calculations and checking for higher symmetry was performed with the PLATON program.^[42]

X-ray Crystal Structure Determination of 3b: $\text{C}_{23}\text{H}_{32}\text{N}_2\text{Rh}_2$; 542.33; red needle; $0.32 \times 0.12 \times 0.08 \text{ mm}^3$; triclinic; $P\bar{1}$ (no. 2); $a = 8.5096(3)$, $b = 10.4024(3)$, $c = 12.9938(4) \text{ \AA}$, $\alpha = 78.8723(11)$, $\beta = 79.4202(11)$, $\gamma = 66.3169(10)^\circ$; $V = 1026.31(6) \text{ \AA}^3$; $Z = 2$; $D_x = 1.755 \text{ g/cm}^3$; $\mu = 1.62 \text{ mm}^{-1}$. 17837 Reflections were measured with a Bruker Kappa ApexII diffractometer with sealed tube and Triumph monochromator ($\lambda = 0.71073 \text{ \AA}$) at a temperature of 150(2) K up to a resolution of $(\sin \theta/\lambda)_{\text{max}} = 0.65 \text{ \AA}^{-1}$. The intensities were integrated with the SAINT software.^[39] Multiscan absorption correction and scaling was performed with SADABS^[40] (correction range 0.67–0.75). 4683 Reflections were unique ($R_{\text{int}} = 0.015$), of which 4343 were observed [$I > 2\sigma(I)$]. The structure was solved with Direct Methods using SIR-97.^[45] Least-squares refinement was performed with SHELXL-97^[41] against F^2 of all reflections. Non-hydrogen atoms were refined freely with anisotropic displacement parameters. All hydrogen atoms were located in difference Fourier maps. The four C–H hydrogen atoms at the coordinated double bonds were refined freely with isotropic displacement parameters. All other hydrogen atoms were refined with a riding model. 180 Parameters were refined with no restraints. R_1/wR_2 [$I > 2\sigma(I)$]: 0.0168/0.0419. R_1/wR_2 [all reflections]: 0.0188/0.0430, $S = 1.026$. Residual electron density between -0.51 and 0.79 e/\AA^3 . Geometry calculations and checking for higher symmetry was performed with the PLATON program.^[42]

X-ray Crystal Structure Determination of 1c: $\text{C}_{22}\text{H}_{28}\text{N}_2\text{Rh}\cdot\text{CH}_3\text{OH}$; 600.39; orange needle; $0.57 \times 0.31 \times 0.13 \text{ mm}^3$; triclinic; $P1$ (no. 1); $a = 7.48444(17)$, $b = 9.5487(2)$, $c = 9.6905(2) \text{ \AA}$, $\alpha = 63.452(1)$, $\beta = 78.364(1)$, $\gamma = 76.874(1)^\circ$; $V = 599.34(2) \text{ \AA}^3$; $Z = 1$; $D_x = 1.663 \text{ g/cm}^3$; $\mu = 0.84 \text{ mm}^{-1}$. 20838 Reflections were measured with a Bruker Kappa ApexII diffractometer with sealed tube and Triumph monochromator ($\lambda = 0.71073 \text{ \AA}$) at a temperature of 150(2) K up to a resolution of $(\sin \theta/\lambda)_{\text{max}} = 0.65 \text{ \AA}^{-1}$. The intensities were integrated with the Eval15 software.^[43] Multiscan absorption correction and scaling was performed with SADABS^[40] (correction range 0.67–0.75). 5430 Reflections were unique ($R_{\text{int}} = 0.013$), of which 5429 were observed [$I > 2\sigma(I)$]. The structure was solved with Direct Methods using SHELXS-97.^[41] Least-squares refinement was performed with SHELXL-97^[41] against F^2 of all reflections. Non-hydrogen atoms were refined freely with anisotropic displacement parameters. All hydrogen atoms were located in difference Fourier maps. The N–H hydrogen and the hydrogen atoms of the cyclooctadiene double bonds were refined freely with isotropic displacement parameters. All other hydrogen atoms were refined with a riding model. 334 Parameters were refined with three restraints (for fixing the origin). R_1/wR_2 [$I > 2\sigma(I)$]: 0.0104/0.0275. R_1/wR_2 [all reflections]: 0.0104/0.0276, $S = 1.061$. Flack parameter^[46] $x = -0.001(8)$. Residual electron density between -0.37 and 0.19 e/\AA^3 . Geometry calculations and checking for higher symmetry was performed with the PLATON program.^[42]

CCDC Crystallographic Data:

CCDC 1429983 (for **1a**), 1429984 (for **1b**), 1429985 (for **2a**), 1429986 (for **3b**), and 1429987 (for **1c**) contain the supplementary crystallographic data for this paper. These data can be obtained free of charge from The Cambridge Crystallographic Data Centre.

DFT Calculations: The gas-phase geometries of complexes **3** and **4** were optimised with the Turbomole program package^[47] coupled to the PQS Baker optimiser^[48] via the BOpt package^[49] at the ri-

DFT^[50]/BP86^[51] level. We used the def2-TZVPP basis set^[52] for all atoms and a small grid (m4), with Grimme's dispersion corrections (disp3 version).^[53] The minima (no imaginary frequencies) were characterised by calculating the Hessian matrix.

Supporting Information (see footnote on the first page of this article): NMR spectra, crystallographic details, computational details.

Acknowledgments

This research was funded by the Netherlands Research Council – Chemical Sciences (NWO-CW) through an ECHO research grant. The Spanish Ministerio de Economía y Competitividad (MINECO) and Fondos Europeos para el Desarrollo Regional (FEDER) (CTQ2014-53033-P) is also acknowledged.

Keywords: Carbenes · Iridium · Ketene · Ligand design · Redox chemistry · Rhodium

- [1] a) J. Choi, A. H. R. MacArthur, M. Brookhart, A. S. Goldman, *Chem. Rev.* **2011**, *111*, 1761–1779; b) G. E. Dobereiner, R. H. Crabtree, *Chem. Rev.* **2010**, *110*, 681–703; c) I. W. C. E. Arends, R. A. Sheldon, in: *Modern Oxidation Methods* (Ed.: J.-E. Bäckvall), Wiley-VCH, Weinheim, Germany, **2004**, p. 83–118; d) M. Beller, C. Bolm, in: *Transition Metals for Organic Synthesis*, 2nd ed., (Ed.: S.-I. Murahashi, Y. Imada), Wiley-VCH, Weinheim, Germany, **2004**, *2*, p. 497–507; e) J. Finney, H.-J. Moon, T. Ronnebaum, M. Lantz, M. Mure, *Arch. Biochem. Biophys.* **2014**, *546*, 19–32; f) D. Rokhsana, E. M. Shepard, D. E. Brown, D. M. Dooley in: *Copper-Oxygen Chemistry* (Eds.: S. Rokita, K. D. Karlin, S. Itoh), Wiley, Hoboken, NJ, USA, **2011**, chapter 3, p. 53–106.
- [2] a) C. Binda, A. Mattevi, D. E. Edmondson, *J. Biol. Chem.* **2002**, *277*, 23973–23976; b) N. S. Scrutton, *Nat. Prod. Rep.* **2004**, *21*, 722–730; c) D. E. Edmondson, C. Binda, A. Mattevi, *Arch. Biochem. Biophys.* **2007**, *464*, 269–276.
- [3] a) G. J. Christian, A. Llobet, F. Maseras, *Inorg. Chem.* **2010**, *49*, 5977–5985; b) J. P. Saucedo-Vázquez, V. M. Ugalde-Saldivar, A. R. Toscano, P. M. H. Kroneck, M. E. Sosa-Torres, *Inorg. Chem.* **2009**, *48*, 1214–1222; c) G. J. Christian, A. Arbuse, X. Fontrodona, M. A. Martinez, A. Llobet, F. Maseras, *Dalton Trans.* **2009**, 6013–6020; d) B. Zhu, M. Lazar, B. G. Trewyna, R. J. Angelici, *J. Catal.* **2008**, *260*, 1–6; e) A. Machkour, D. Mandon, M. Lachkar, R. Welter, *Eur. J. Inorg. Chem.* **2005**, 158–161; f) V. Amendola, L. Fabbrizzi, E. Mundum, P. Pallavicini, *Dalton Trans.* **2003**, 773–774; g) X. Gu, W. Chen, D. Morales-Morales, C. M. Jensen, *J. Mol. Catal. A* **2002**, *189*, 119–124; h) F. R. Keene, *Coord. Chem. Rev.* **1999**, *187*, 121–149.
- [4] C. Zhang, N. Jiao, *Angew. Chem. Int. Ed.* **2010**, *49*, 6174–6177; *Angew. Chem.* **2010**, *122*, 6310.
- [5] a) S. Aiki, A. Taketoshi, J. Kuwabara, T. Koizumi, T. Kanbara, *J. Organomet. Chem.* **2011**, *696*, 1301–1304; b) A. Taketoshi, T. Koizumi, T. Kanbara, *Tetrahedron Lett.* **2010**, *51*, 6457–6459; c) W. H. Bernskoetter, M. Brookhart, *Organometallics* **2008**, *27*, 2036–2045; d) K. Yamaguchi, N. Mizuno, *Angew. Chem. Int. Ed.* **2003**, *42*, 1480–1483; *Angew. Chem.* **2003**, *115*, 1518.
- [6] a) R. E. Rodríguez-Lugo, M. Trincado, M. Vogt, F. Tewes, G. Santiso-Quinones, H. Grützmacher, *Nat. Chem.* **2013**, *5*, 342–347; for a reversed example of active catalyst formation involving imine-to-amine-type ligand transformation, see: b) A. Mikhailine, M. I. Maishan, A. J. Lough, R. H. Morris, *J. Am. Chem. Soc.* **2012**, *134*, 12266–12280.
- [7] See refs.^[5c,5d] and: a) C. Jun, K. Chung, J. Hong, *Org. Lett.* **2001**, *3*, 301–303; b) O. Saidi, A. J. Blacker, M. M. Farah, S. P. Marsden, J. M. J. Williams, *Angew. Chem. Int. Ed.* **2009**, *48*, 7375–7378; *Angew. Chem.* **2009**, *121*, 7511; c) W. P. Gri, B. Reddy, A. G. F. Shoair, M. Suriaatmaja, A. J. P. White, D. J. Williams, *J. Chem. Soc., Dalton Trans.* **1998**, *2*, 2819–2825.
- [8] a) K. T. Tseng, A. M. Rizzi, N. K. Szymczak, *J. Am. Chem. Soc.* **2013**, *135*, 16352–16355; b) D. Talwar, A. Gonzalez-de-Castro, H. Y. Li, J. Xiao, *Angew. Chem. Int. Ed.* **2015**, *54*, 5223–5227; *Angew. Chem.* **2015**, *127*, 5312; c) S. Muthaiah, S. H. Hong, *Adv. Synth. Catal.* **2012**, *354*, 3045–3053.
- [9] a) F. R. Keene, M. J. Ridd, M. R. Snow, *J. Am. Chem. Soc.* **1983**, *105*, 7075–7081; b) J. P. Saucedo-Vázquez, V. M. Ugalde-Saldivar, A. R. Toscano, P. M. H. Kroneck, M. E. Sosa-Torres, *Inorg. Chem.* **2009**, *48*, 1214–1222; c) G. J. Christian, A. Arbuse, X. Fontrodona, M. A. Martinez, A. Llobet, F. Maseras, *Dalton Trans.* **2009**, 6013–6020.
- [10] J. Gómez, G. García-Herbosa, J. V. Cuevas, A. Arnáiz, A. Carbayo, A. Muñoz, L. Falvello, P. E. Fanwick, *Inorg. Chem.* **2006**, *45*, 2483–2493.
- [11] G. J. Christian, A. Llobet, F. Maseras, *Inorg. Chem.* **2010**, *49*, 5977–5985.
- [12] a) W. Kaim, *Inorg. Chem.* **2011**, *50*, 9752–9765; b) V. Lyaskovskyy, B. de Bruin, *ACS Catal.* **2012**, *2*, 270–279; c) J. I. van der Vlugt, *Eur. J. Inorg. Chem.* **2012**, 363–375; d) V. K. K. Praneeth, M. R. Ringenberg, T. R. Ward, *Angew. Chem. Int. Ed.* **2012**, *51*, 10228–10234; *Angew. Chem.* **2012**, *124*, 10374; e) O. R. Luca, R. H. Crabtree, *Chem. Soc. Rev.* **2013**, *42*, 1440–1459; f) D. L. J. Broere, R. Plessius, J. I. van der Vlugt, *Chem. Soc. Rev.* **2015**, *44*, 6886–6915.
- [13] a) B. de Bruin, T. P. J. Peters, N. N. F. A. Suos, D. Gelder, J. M. M. Smits, A. W. Gal, *Inorg. Chim. Acta* **2002**, *337*, 154–162; b) D. G. H. Hetterscheid, B. de Bruin, J. M. M. Smits, A. W. Gal, *Organometallics* **2003**, *22*, 3022–3024; c) D. G. H. Hetterscheid, M. Klop, R. J. N. A. M. Kicken, J. M. M. Smits, E. J. Reijerse, B. de Bruin, *Chem. Eur. J.* **2007**, *13*, 3386–3405; d) C. Tejel, M. A. Ciriano, M. P. del Río, D. G. H. Hetterscheid, N. Tschlis i Spithas, J. M. M. Smits, B. de Bruin, *Chem. Eur. J.* **2008**, *14*, 10932–10936; e) C. Tejel, M. P. del Río, M. A. Ciriano, E. J. Reijerse, F. Hartl, S. Zális, D. G. H. Hetterscheid, N. Tschlis i Spithas, B. de Bruin, *Chem. Eur. J.* **2009**, *15*, 11878–11889.
- [14] a) T. Büttner, J. Geier, G. Frison, J. Harmer, C. Calle, A. Schweiger, H. Schönberg, H. Grützmacher, *Science* **2005**, *307*, 235–238; b) P. Maire, M. Königsmann, A. Sreekanth, J. Harmer, A. Schweiger, H. Grützmacher, *J. Am. Chem. Soc.* **2006**, *128*, 6578–6580; c) Y. Miyazato, T. Wada, K. Tanaka, *Bull. Chem. Soc. Jpn.* **2006**, *79*, 745–747; d) Y. Miyazato, T. Wada, J. T. Muckerman, E. Fujita, K. Tanaka, *Angew. Chem. Int. Ed.* **2007**, *46*, 5728–5730; *Angew. Chem.* **2007**, *119*, 5830.
- [15] a) C. Tejel, M. A. Ciriano, M. P. del Río, F. J. van den Bruele, D. G. H. Hetterscheid, N. Tschlis i Spithas, B. de Bruin, *J. Am. Chem. Soc.* **2008**, *130*, 5844–5845; b) C. Tejel, M. P. del Río, L. Asensio, F. J. van den Bruele, M. A. Ciriano, N. Tschlis i Spithas, D. G. H. Hetterscheid, B. de Bruin, *Inorg. Chem.* **2011**, *50*, 7524; c) C. Tejel, L. Asensio, M. P. del Río, M. A. Ciriano, B. de Bruin, J. A. López, M. A. Ciriano, *Eur. J. Inorg. Chem.* **2012**, 512; d) C. Tejel, L. Asensio, M. A. Ciriano, J. A. López, B. de Bruin, M. P. del Río, *Angew. Chem. Int. Ed.* **2011**, *50*, 8839; *Angew. Chem.* **2011**, *123*, 9001; e) Z. Tang, E. Otten, J. N. H. Reek, J. I. van der Vlugt, B. de Bruin, *Chem. Eur. J.* **2015**, *21*, 12683–12693.
- [16] a) J. I. van der Vlugt, J. N. H. Reek, *Angew. Chem. Int. Ed.* **2009**, *48*, 8832–8846; *Angew. Chem.* **2009**, *121*, 8990; b) J. R. Khusnutdinova, D. Milstein, *Angew. Chem. Int. Ed.* **2015**, *54*, 12236–12273. For specific examples with Rh and Ir, see: c) M. Feller, Y. Diskin-Posner, L. J. W. Shimon, E. Ben-Ari, D. Milstein, *Organometallics* **2012**, *31*, 4083–4101; d) M. Feller, A. Karton, G. Leitus, J. M. L. Martin, D. Milstein, *J. Am. Chem. Soc.* **2006**, *128*, 12400–12401; e) M. Feller, E. Ben-Ari, Y. Diskin-Posner, R. Carmieli, L. Weiner, D. Milstein, *J. Am. Chem. Soc.* **2015**, *137*, 4634–4637. See also: f) Y. Gloaguen, C. Rebreyend, M. Lutz, P. Kumar, M. Huber, J. I. van der Vlugt, S. Schneider, B. de Bruin, *Angew. Chem. Int. Ed.* **2014**, *53*, 6814–6818; *Angew. Chem.* **2014**, *126*, 6932.
- [17] For oxidative loss of H₂ in PNP ligands with aliphatic backbones, see: a) M. Käß, A. Friedrich, M. Drees, S. Schneider, *Angew. Chem. Int. Ed.* **2009**, *48*, 905–907; *Angew. Chem.* **2009**, *121*, 922; b) A. Friedrich, M. Drees, M. Käss, E. Herdtweck, S. Schneider, *Inorg. Chem.* **2010**, *49*, 5482–5494.
- [18] Z. Tang, S. Mandal, N. D. Paul, M. Lutz, P. Li, J. I. van der Vlugt, B. de Bruin, *Org. Chem. Front.* **2015**, *2*, 1561–1577.
- [19] A triplet-like doublet of doublet with two small *J* constants close in value (1.3–1.5 Hz), presumably one is ³J_{Rh,H} and the second is ³J_{H,H} corresponding to coupling with the C–H of the methyl group.
- [20] C. Tejel, J. M. Villoro, M. A. Ciriano, J. A. López, E. Eguizabal, F. J. Lahoz, V. I. Bakhmutov, L. A. Oro, *Organometallics* **1996**, *15*, 2967–2978.
- [21] The short distance of Rh2–C6 may indicate a σ-bond between the two atoms and thus an sp³ carbon, but an almost square-planar bonding geometry was found around C6 with N2, H6 and C5 [∠N2–C6–C5 116.36(14)°, ∠C5–C6–H6 119.7(12)°, ∠H6–C6–N2 123.1(12)°, ∑ = 359.2(17)°], pointing to an sp²-hybridized carbon atom.

- [22] A more localised charge distribution is also found on the ligand in **3b** than in **C2**, and the Rh2 in **3b** coordinates to an N2–C6–C5 “azaallyl” moiety (Figure 3, **III**), which is different from that in complex **C2**. The rhodium (Rh1 in **3b**) is less capable to induce and stabilise a charge-delocalised M–N2–C6–C5–N1 metallocycle than iridium (Ir1 in **C2**). The longer N1=C5 and N2=C6 bond lengths in **3b** compared with those in **C2** reflect this difference (N1=C5: 1.385(2) vs. 1.394(5), N2=C6: 1.387(2) vs. 1.396(5) Å, for **1b** and **C2**, respectively).
- [23] a) S. Takemoto, S. Otsuki, Y. Hashimoto, K. Kamikawa, H. Matsuzaka, *J. Am. Chem. Soc.* **2008**, *130*, 8904–905; b) S.-Y. Liu, I. D. Hills, G. C. Fu, *Organometallics* **2002**, *21*, 4323–4325; c) A. S. Batsanov, V. G. Andrianov, Y. T. Struchkov, V. S. Khandkarova, A. Z. Rubezhov, *Metalloorg. Khim.* **1988**, *1*, 68.
- [24] a) H. Staudinger, *Ber. Dtsch. Chem. Ges.* **1905**, *38*, 1735–1739; b) T. T. Tidwell, *Eur. J. Org. Chem.* **2006**, 563–576; c) D. H. Paull, A. Weatherwax, T. Lectka, *Tetrahedron* **2009**, *65*, 6771–6803; d) A. D. Allen, T. T. Tidwell, *Eur. J. Org. Chem.* **2012**, 1081–1096; e) A. D. Allen, T. T. Tidwell, *Chem. Rev.* **2013**, *113*, 7287–7342.
- [25] a) N. Ungvári, F. Ungváry, *Carbonylation of Diazoalkanes*, in: *Modern Carbonylation Methods* (Ed.: L. Kollár), Wiley-VCH, Weinheim, Germany, **2008**, chapter 8, p. 199–221; b) K. H. Dötz, J. Stendel, *Chem. Rev.* **2009**, *109*, 3227–3274.
- [26] Conventional synthetic methods generally have limitations such as narrow substrate scope, strictly controlled conditions and generation of detrimental side products, such as thermolysis of ketene dimers, see: a) H. W. Moore, D. S. Wilbur, *J. Org. Chem.* **1980**, *45*, 4483–4491; for Wolff rearrangement, see: b) Y. Chiang, A. J. Kresge, V. V. Popik, *J. Am. Chem. Soc.* **1999**, *121*, 5930–5932; c) B. D. Wagner, B. R. Arnold, G. S. Brown, J. Luszytk, *J. Am. Chem. Soc.* **1998**, *120*, 1827–1834; for dehydrohalogenation of acyl halide precursors, see: d) L. S. Hegedus, J. Montgomery, Y. Narukawa, D. C. Snustad, *J. Am. Chem. Soc.* **1991**, *113*, 5784–5791.
- [27] a) K. H. Dötz, J. Mühlemeier, *Angew. Chem. Int. Ed. Engl.* **1982**, *21*, 929–933; *Angew. Chem.* **1982**, *94*, 936; b) P. T. Barger, B. D. Santarsiero, J. Armantrout, J. E. Bercaw, *J. Am. Chem. Soc.* **1984**, *106*, 5178–5186; c) N. Ungvári, E. Fördös, J. Balogh, T. Kégl, L. Párkányi, F. Ungváry, *Organometallics* **2010**, *29*, 3837–3851.
- [28] a) T. Ye, M. A. Mckervey, *Chem. Rev.* **1994**, *94*, 1091–1160; b) R. Tuba, F. Ungváry, *J. Mol. Catal. A* **2003**, *203*, 59–67; c) Z. Zhang, J. Wang, *Tetrahedron* **2008**, *64*, 6577–6605; d) E. Fördös, R. Tuba, L. Párkányi, T. Kégl, F. Ungváry, *Eur. J. Org. Chem.* **2009**, 1994–2002; e) N. D. Paul, A. Chirila, H. Lu, X. P. Zhang, B. de Bruin, *Chem. Eur. J.* **2013**, *19*, 12953–12958; f) Z. Zhang, Y. Liu, L. Ling, Y. Li, Y. Dong, M. Gong, X. Zhao, Y. Zhang, J. Wang, *J. Am. Chem. Soc.* **2011**, *133*, 4330–4341; g) Q. Xiao, Y. Zhang, J. Wang, *Acc. Chem. Res.* **2013**, *46*, 236–247.
- [29] C. R. Pitts, T. Lectka, *Chem. Rev.* **2014**, *114*, 7930–7953.
- [30] a) P. Schwab, N. Mahr, J. Wolf, H. Werner, *Angew. Chem. Int. Ed. Engl.* **1993**, *32*, 1480–1482; *Angew. Chem.* **1993**, *105*, 1498; b) H. Werner, P. Schwab, E. Bleuel, N. Mahr, B. Windmüller, J. Wolf, *Chem. Eur. J.* **2000**, *6*, 4461–4470.
- [31] However, complex **1b** does not show dehydrogenation activity for the related amine substrates under similar conditions, indicating fast dehydrogenation of the intermediate amino/amido species **8b** might also derive from other reactions, e.g. transimination between hydrolyzed **4b** and **5**.
- [32] a) R. B. Morin, M. Gorman, *Chemistry and Biology of β -Lactam Antibiotics*, 6th Ed., Academic Press, New York, **1982**; b) B. Alcaide, P. Almendros, C. Aragoncillo, *Chem. Rev.* **2007**, *107*, 4437–4492; c) T. T. Tidwell, *Angew. Chem. Int. Ed.* **2008**, *47*, 1016–1020; *Angew. Chem.* **2008**, *120*, 1032; d) N. A. A. El-Kanzi, *Heterocycl. Lett.* **2013**, *3*, 81–109; e) A. Gupta, A. K. Halve, *Int. J. Pharm. Sci. Res.* **2015**, *6*, 978–987.
- [33] a) M. Staudinger, *Justus Liebigs Ann. Chem.* **1907**, *356*, 51–123; b) G. I. Georg, V. T. Ravikumar, in: *The Organic Chemistry of β -Lactams* (Ed.: G. I. Georg), Verlag Chemie, New York, **1993**, p. 295–398; c) Palomo, J. M. Aizpurua, I. Ganboa, M. Oiarbide, *Curr. Med. Chem.* **2004**, *11*, 1837–1872; d) R. Tuba, *Org. Biomol. Chem.* **2013**, *11*, 5976–5988.
- [34] The *cis-trans* stereoselectivity has been a less well understood and controversial topic in the Staudinger reaction, and many factors have been observed to affect the selectivity, see: a) L. S. Hegedus, J. Montgomery, Y. Narukawa, D. C. Snustad, *J. Am. Chem. Soc.* **1991**, *113*, 5784–5791; b) S. France, A. Weatherwax, A. E. Taggi, T. Lectka, *Acc. Chem. Res.* **2004**, *37*, 592–600; c) Y. Wang, Y. Liang, L. Jiao, D. M. Du, J. Xu, *J. Org. Chem.* **2006**, *71*, 6983–6990; d) B. K. Banik, B. Lecea, A. Arrieta, A. De Cózar, F. P. Cossío, *Angew. Chem. Int. Ed.* **2007**, *46*, 3028–3032; *Angew. Chem.* **2007**, *119*, 3088; e) F. P. Cossío, A. Arrieta, M. a. Sierra, *Acc. Chem. Res.* **2008**, *41*, 925–936; f) H. Qi, X. Li, J. Xu, *Org. Biomol. Chem.* **2011**, *9*, 2702–2714.
- [35] C. R. Pitts, T. Lectka, *Chem. Rev.* **2014**, *114*, 7930–7953.
- [36] G. Giordano, R. H. Crabtree, *Inorg. Synth.* **1990**, *28*, 88–90.
- [37] R. Uson, L. A. Oro, J. A. Cabeza, *Inorg. Synth.* **1985**, *23*, 126–129.
- [38] B. de Bruin, J. A. Brands, J. J. M. Donners, M. P. J. Donners, R. de Gelder, J. M. M. Smits, A. W. Gal, A. L. Spek, *Chem. Eur. J.* **1999**, *5*, 2921–2936.
- [39] SAINTE, Bruker AXS Inc., Madison, Wisconsin, USA, **2007**.
- [40] G. M. Sheldrick, SADABS, University of Göttingen, Germany, **2008**.
- [41] G. M. Sheldrick, *Acta Crystallogr., Sect. A* **2008**, *64*, 112–122.
- [42] A. L. Spek, *Acta Crystallogr., Sect. D* **2009**, *65*, 148–155.
- [43] A. M. M. Schreurs, X. Xian, L. M. J. Kroon-Batenburg, *J. Appl. Crystallogr.* **2010**, *43*, 70–82.
- [44] P. T. Beurskens, G. Beurskens, R. de Gelder, S. Garcia-Granda, R. O. Gould, J. M. M. Smits, *DIRDIF-08*, Crystallography Laboratory, University of Nijmegen, The Netherlands, **2008**.
- [45] A. Altomare, M. C. Burla, M. Camalli, G. L. Cascarano, C. Giacovazzo, A. Guagliardi, A. G. G. Moliterni, G. Polidori, R. Spagna, *J. Appl. Crystallogr.* **1999**, *32*, 115–119.
- [46] H. D. Flack, *Acta Crystallogr., Sect. A* **1983**, *39*, 876–881.
- [47] R. Ahlrichs, *Turbomole*, version 6.5, *Theoretical Chemistry Group*, University of Karlsruhe, Germany.
- [48] PQS, version 2.4, Parallel Quantum Solutions, Fayetteville, Arkansas, USA, **2001**; the Baker optimizer is available separately from PQS upon request, see: I. Baker, *J. Comput. Chem.* **1986**, *7*, 385–395.
- [49] P. H. M. Budzelaar, *J. Comput. Chem.* **2007**, *28*, 2226–2236.
- [50] M. Sierka, A. Hogeckamp, R. Ahlrichs, *J. Chem. Phys.* **2003**, *118*, 9136–9148.
- [51] a) A. D. Becke, *Phys. Rev. A* **1988**, *38*, 3098–3100; b) J. P. Perdew, *Phys. Rev. B* **1986**, *33*, 8822–8824.
- [52] a) F. Weigend, R. Ahlrichs, *Phys. Chem. Chem. Phys.* **2005**, *7*, 3297–3305; b) F. Weigend, M. Häser, H. Patzelt, R. Ahlrichs, *Chem. Phys. Lett.* **1998**, *294*, 143–152.
- [53] S. Grimme, J. Antony, S. Ehrlich, H. Krieg, *J. Chem. Phys.* **2010**, *132*, 154104.

Received: November 9, 2015

Published Online: January 25, 2016